AGU PUBLICATIONS

JGR

Journal of Geophysical Research: Oceans

RESEARCH ARTICLE

10.1002/2014JC010019

Key Points:
- Direct current measurements in the southwestern subpolar North Atlantic
- North Atlantic Current (NAC) transports 110 Sv, 75 Sv recirculating locally
- Deep Western Boundary Current transports 30 Sv, 15 Sv recirculating into NAC

Correspondence to:
C. Mertens,
cmertens@uni-bremen.de

Citation:
Mertens, C., M. Rhein, M. Walter, C. W. Böning, E. Behrens, D. Kieke, R. Steinfeldt, and U. Stöber (2014), Circulation and transports in the Newfoundland Basin, western subpolar North Atlantic, *J. Geophys. Res. Oceans*, *119*, 7772–7793, doi:10.1002/2014JC010019.

Received 3 APR 2014
Accepted 20 OCT 2014
Accepted article online 25 OCT 2014
Published online 19 NOV 2014

Circulation and transports in the Newfoundland Basin, western subpolar North Atlantic

Christian Mertens[1], Monika Rhein[1], Maren Walter[1], Claus W. Böning[2], Erik Behrens[2], Dagmar Kieke[1], Reiner Steinfeldt[1], and Uwe Stöber[1]

[1]University of Bremen, Institute of Environmental Physics, Bremen, Germany, [2]GEOMAR Helmholtz Centre for Ocean Research Kiel, Kiel, Germany

Abstract The southwestern part of the subpolar North Atlantic east of the Grand Banks of Newfoundland and Flemish Cap is a crucial area for the Atlantic Meridional Overturning Circulation. Here the exchange between subpolar and subtropical gyre takes place, southward flowing cold and fresh water is replaced by northward flowing warm and salty water within the North Atlantic Current (NAC). As part of a long-term experiment, the circulation east of Flemish Cap has been studied by seven repeat hydrographic sections along 47°N (2003–2011), a 2 year time series of current velocities at the continental slope (2009–2011), 19 years of sea surface height, and 47 years of output from an eddy resolving ocean circulation model. The structure of the flow field in the measurements and the model shows a deep reaching NAC with adjacent recirculation and two distinct cores of southward flow in the Deep Western Boundary Current (DWBC): one core above the continental slope with maximum velocities at mid-depth and the second farther east with bottom-intensified velocities. The western core of the DWBC is rather stable, while the offshore core shows high temporal variability that in the model is correlated with the NAC strength. About 30 Sv of deep water flow southward below a density of $\sigma_\theta = 27.68$ kg m^{-3} in the DWBC. The NAC transports about 110 Sv northward, approximately 15 Sv originating from the DWBC, and 75 Sv recirculating locally east of the NAC, leaving 20 Sv to be supplied by the NAC from the south.

1. Introduction

The Atlantic meridional overturning circulation at the boundary between the subpolar and subtropical gyre is a mainly horizontal cell. Cold and fresh water flows southward in a deep reaching boundary current along the continental margin east of the Grand Banks of Newfoundland, that is compensated by an adjacent northward flow that carries warm and salty water within the upper layer [e.g., *Meinen and Watts*, 2000; *Rhein et al*., 2011; *Schott et al*., 2004]. These strong currents and their interchange control the deep water export from the subpolar gyre [e.g., *Bower et al*., 2009; *Kieke et al*., 2009; *Lozier et al*., 2013].

The North Atlantic Current (NAC) is the northern extension of the Gulf Stream [e.g., *Rossby*, 1996]. The Gulf Stream has its maximum eastward transport of 150 Sv at 60°W [*Hogg*, 1992]. At the southeastern tip of the Grand Banks of Newfoundland part of it recirculates or continues in an eastern direction, while the remaining fraction turns northward, now called the NAC. On its way north, the NAC follows the continental margin roughly along the 4000 m isobath, thereby forming a number of small recirculation cells [*Rossby*, 1996], to the so-called Northwest Corner at approximately 52°N, where it turns eastward (Figure 1). At the Mid-Atlantic Ridge, the path of the NAC aligns with the Charlie-Gibbs Fracture Zone (53°N), the Faraday Fracture Zone (50°N), and/or the Maxwell Fracture Zone (48°N), carrying a total transport of about 30 Sv into the eastern basin [e.g., *Rhein et al*., 2011]. Altimeter data from 1992 to 2006 show that the NAC often splits up into branches, with the main pathway alternating between 53°N and 49°N [*Bower and von Appen*, 2008]. Since 2006, the NAC has preferred the two southern pathways and was infrequently observed at 53°N [*Roessler*, 2013].

The part of the NAC that remains in the western North Atlantic recirculates within the Newfoundland Basin [e.g., *Schmitz and McCartney*, 1993]. Evidence for such a southward recirculation east of the NAC, possibly in the form of a chain of semipermanent eddies east of the Grand Banks [*Krauss*, 1986; *Käse and Krauss*, 1996], was found in deep float as well as surface drifter trajectories [*Reverdin et al*., 2003; *Bower et al*., 2002] and

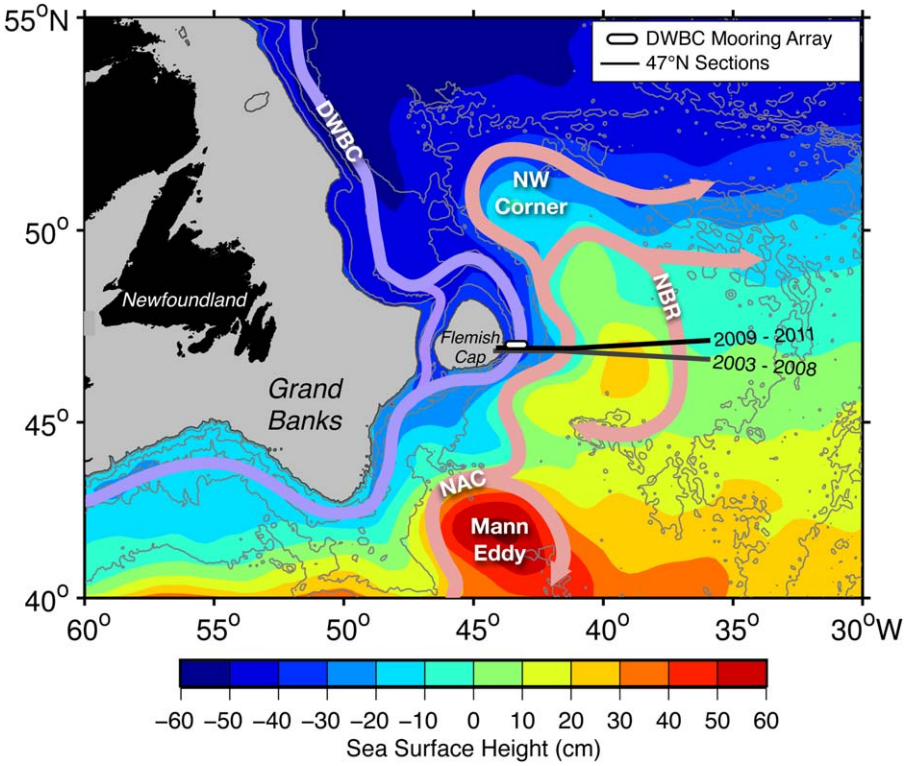

Figure 1. Average absolute dynamic topography gridded on 1/3° from AVISO, bathymetry of the Newfoundland Basin, and schematic depiction of the circulation: southward flowing Deep Western Boundary Current (DWBC), northward flowing North Atlantic Current (NAC), and recirculation in the Newfoundland Basin (NBR). Arrows indicate mean paths of the DWBC and NAC. Hydrographic sections are shown as black lines. Also indicated is the position of the array of three closely spaced moorings in the DWBC.

dubbed the Newfoundland Basin Recirculation Gyre [NBR, *Bower et al*., 2009]. In their analysis of observations and results from the 1/12° FLAME model, *Rhein et al*. [2011] found that the fluctuations of the northward volume transport of the overturning circulation were dominated by variability west of the Mid-Atlantic Ridge. In the model, the strongest variability in the western basin was caused by meandering of the front between the southward flowing boundary current and the northward NAC.

The export of cold water from the subpolar gyre follows several pathways. The majority of the water is carried south within the Deep Western Boundary Current (DWBC) along the continental margin; it splits up north of 47°N, with one shallow branch flowing through Flemish Pass, mainly carrying (upper) Labrador Sea Water [*Rhein et al*., 2011], and the other east of Flemish Cap. Further south, at the southeastern tip of the Grand Banks, a deep water transport between 12.9 Sv [*Schott et al*., 2004, from moored current meters] and 17.5 Sv [*Schott et al*., 2006, from combined LADCP sections] was observed. Evidence for additional interior pathways of deep water export comes from mooring data close to the Mid-Atlantic Ridge, where occasional southward flow was observed in the Labrador Sea Water layer [*Kieke et al*., 2009]. The further exchange between the DWBC and the interior is evident in an anomalous decline of chlorofluorocarbons within the boundary current between 47°N and 42°N [*Rhein et al*., 2002]. The interior pathways are likely sustained by a series of recirculation cells along the western boundary [*Gary et al*., 2011].

Here we analyze observations along a zonal section at 47°N that crosses the DWBC and the NAC, using shipboard and moored measurements, satellite altimetry, and output of the VIKING20 eddy resolving ocean circulation model [*Behrens*, 2013] to quantify transports and their variability in the Newfoundland Basin as well as to study the interaction between the boundary current and the interior. The paper is organized as follows: after the introduction, the shipboard and mooring data, the altimetry data, and the model configuration are presented. In section 3, we describe the hydrography and flow field from the observations, the synoptic variability, and the time-averaged transports. In section 4, the variability on intraseasonal to interannual timescales is analyzed. Finally, the results are discussed and a regional budget of volume transports is derived in section 5.

Table 1. CTD/LADCP Stations Along the 47°N Section Between Flemish Cap and 36°W on Seven Cruises Between 2003 and 2011

Cruise	Date	No. of Stations
Meteor 59/2	16–26 August 2003	24
Thalassa SUBPOLAR	5–16 June 2005	10(3)[a]
Maria S. Merian 5/1	28–30 April 2007	13[b]
Maria S. Merian 9/1	4–10 August 2008	21
Maria S. Merian 12/3	30 July to 5 August 2009	16
Meteor 82/2	6–28 August 2010	19
Meteor 85/1	25 June to 16 July 2011	17

[a]No stations between 43 and 41°W due to severe weather conditions, only 3 stations with LADCP because of technical problems.
[b]No stations east of 41°W.

2. Data

The circulation and water mass properties east of Flemish Cap were studied using (1) shipboard measurements, (2) mooring data, (3) altimetry, and (4) model output. The seven repeat hydrographic sections along 47°N were obtained between the years 2003 and 2011, the 2 year long-time series of current velocity at the continental slope of Flemish Cap between summer 2009 and summer 2011 (Figure 1). Altimetry was used for the period from 1993 to 2012, and model results with realistic forcing from 1960 to 2007.

2.1. Shipboard Measurements

The hydrographic observations were carried out on three mooring deployment and recovery cruises as well as on four earlier cruises (Table 1). On the later three cruises, the stations were placed slightly north compared to the earlier cruises (Figure 1). The section was fully occupied between the Flemish Cap and 36°W during five of the cruises, with a total number of stations between 16 and 24 (Table 1). During the *Maria S. Merian* cruise 5/1, for technical reasons, it was only possible to complete 13 stations within the boundary current west of 41°W. On the cruise SUBPOLAR with the French vessel *Thalassa*, only 10 stations were carried out, with no stations in the deep part of the western boundary current due to severe weather conditions. On most of the cruises, the section continued eastward across the Mid-Atlantic Ridge and toward the European continental slope [*Rhein et al*., 2011]. Here we consider only the data west of 36°W, focussing on the region dominating the flow field, the transports, and their variability in the Newfoundland Basin.

On each cruise, a Sea-Bird Electronics SBE 9/11plus system was used for conductivity-temperature-depth (CTD) casts. Salinity was calibrated using water samples from Niskin bottles. The calibrated salinities fall within ± 0.002 of the bottle salinities.

Currents were measured by lowering two acoustic Doppler current profilers (ADCP), one upward and one downward looking, together with the CTD at each station along the section. The instruments used were Teledyne RDI 300 kHz Workhorse Monitor ADCPs operated in synchronized mode at a ping rate of 1 Hz and 10 m depth bins. The raw data were processed as described by *Visbeck* [2002] yielding full depth profiles of horizontal velocity with a vertical resolution of 10 m.

Shipboard ADCP data were collected on all cruises using different instruments, on *Maria S. Merian* and *Meteor* TRDI Ocean Surveyor with either 75 or 38 kHz, on *Thalassa* a 75 kHz RDI narrowband ADCP. The vertical range was up to 1400 m for the 38 kHz instrument and 600–700 m for the 75 kHz instruments, the vertical resolution 32 or 16 m for these frequencies, respectively. The error of 5 km mean velocities, averaged along the ship's track, ranges from 2 to 3.5 cm s^{-1}, depending on instrument type.

The lowered ADCP measurements from the different cruises were interpolated onto a regular grid with 10 m vertical resolution and a horizontal spacing that varies smoothly from 4 km at the continental slope to 40 km in the basin interior. Density was interpolated onto the same grid. Transports of the boundary current, NAC, and NBR were then calculated from the individual sections in longitudinal bands; we discriminate between a total transport, which denotes the northward or southward transport of a current core or density layer, and the net transport, which denotes the residual between the northward and southward transport in a layer. In terms of longitudinal extent, the DWBC is defined as the southward flow west of 41°W, the NAC is the northward flow west of 38.5°W, and the NBR constitutes of the southward flow between 37°W and 41°W.

The lowered ADCP data were detided using the TPXO7.2 tidal model [*Egbert and Erofeeva*, 2002]. The maximum amplitude of the tidal velocities is largest slightly inshore of 43°W, where it reaches up to 4 cm s^{-1}, falls below 2 cm s^{-1} at 42°W and decreases further offshore. The effect on the calculated transport is small, generally less than 1 Sv or 0.5%.

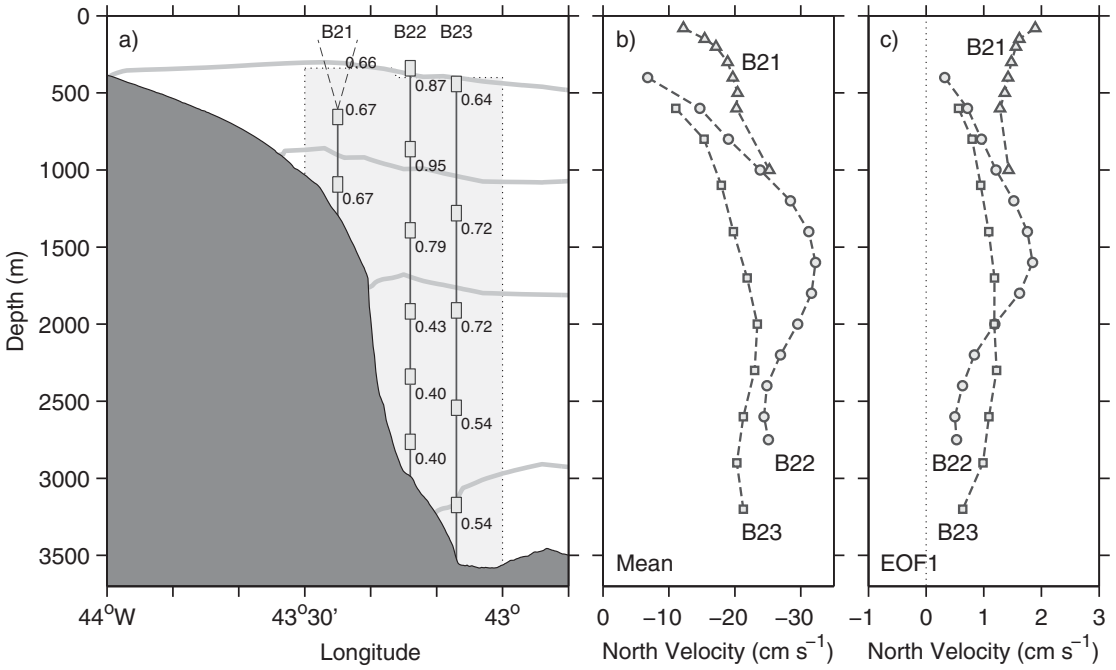

Figure 2. (a) Schematic of Deep Western Boundary Current mooring array (deployment 2009–2010), indicating the nominal depths of current meters (cf. Table 2). Numbers denote the correlation coefficients between the boundary current transport and individual velocity time series. Light gray contours indicate isopycnals separating different water masses, bathymetry (dark gray) from shipboard multibeam echosounder. Light shading indicates total area for DWBC transport calculations. (b) Mean of gridded meridional velocities from first deployment period, interpolated using the first five EOFs (see text for details). (c) First EOF.

2.2. Moorings

An array of three closely spaced current meter moorings (Figure 2a and Table 2) was deployed at the steep continental slope off Flemish Cap to measure the volume transport of the DWBC and its variability, with the central mooring (B22) placed in the velocity maximum of the DWBC. The Flemish Cap mooring array is part of an observational program carried out to study the variability of circulation in the Newfoundland Basin in relation to the NAC transport across the Mid-Atlantic Ridge [*Rhein et al.*, 2011].

The first deployment of the moorings was during the *Maria S. Merian* cruise 12/3 by the end of July 2009. The moorings were recovered on the *Meteor* cruise 82/2 on 7 August 2010 and redeployed a few days later. After the second year, only the two westernmost moorings could be recovered on the *Meteor* cruise 85/1 in mid July 2011, while the third mooring (B23) was lost.

The current meters used in the moorings were one TRDI Instruments 75 kHz WorkHorse ADCP (Long Ranger), three Sontek Argonauts, and nine Aanderaa recording current meters with Doppler sensor (RCM 11). Ten of the current meters were equipped with pressure sensors to measure the instrument depth. The precision of the RCM 11 current meters is of about 0.5 cm s^{-1} according to the manufacturer. For the Argonauts, an averaging interval of 120 seconds and a cell size of 3 m were used which results in a nominal velocity precision of 1.1 cm s^{-1}. The ADCPs were used with a cell size of 16 m and 21 pings per ensemble that results a standard deviation of velocity measurements of 1.65 cm s^{-1}. The sampling interval was 60 min for ADCP and RCM, and 20 min for the Argonauts. The instruments delivered full data records except for three of the RCM11 and the Argonauts, that suffered battery problems and, in case of one instrument, flooding, all of which resulted in truncated data records (Table 2 and Figure 3).

The strong currents in the DWBC caused severe mooring motion and displacement of instruments of several hundreds of meters from their nominal depth. Thus it is necessary to interpolate the measurements on fixed depths between the individual velocity time series (Figures 2b). To this end, the time series were 40 h low-pass filtered and daily subsampled. A new depth grid was defined for each mooring, and the measured time series from the first year of deployment were linearly interpolated onto this grid. Empirical orthogonal functions (EOFs) were constructed to fill the gaps in the moored time series caused by mooring motion or

Table 2. Positions and Deployment Periods of DWBC Moorings at Flemish Cap Between 2009 and 2011[a]

Mooring	Position Water Depth	Nominal Depth (m)	Instrument Type	Sampling Interval (min)	Start and End Date
B21-1	47° 06.05′ N	656	WH75	60	31 Jul 2009–7 Aug 2010
	43° 25.00′ W	1094	ARG	20	31 Jul 2009–7 Jul 2010
	1295 m				
B21-2	47° 06.00′ N	582	WH75	60	10 Aug 2010–15 Jul 2011
	43° 24.97′ W	1042	ARG	20	10 Aug 2010–25 Apr 2011
	1295 m				
B22-1	47° 05.85′ N	340	RCM11	60	31 Jul 2009–7 Aug 2010
	43° 14.18′ W	865	RCM11	60	31 Jul 2009–7 Aug 2010
	2980 m	1391	RCM11	60	31 Jul 2009–7 Aug 2010
		1917	RCM11	60	31 Jul 2009–7 Aug 2010
		2340	RCM11	60	31 Jul 2009–7 Aug 2010
		2763	ARG	20	31 Jul 2009–29 Apr 2010
B22-2	47° 06.30′ N	325	RCM11	60	10 Aug 2010–13 Jul 2011
	43° 13.85′ W	852	RCM11	60	10 Aug 2010–25 Jan 2011
	3000 m	1484	RCM11	60	10 Aug 2010–13 Jul 2011
		2117	RCM11	60	10 Aug 2010–12 Sep 2010
		2749	ARG	20	10 Aug 2010–12 Apr 2011
B23-1	47° 06.00′ N	442	RCM11	60	31 Jul 2009–7 Aug 2010
	43° 07.19′ W	1280	RCM11	60	31 Jul 2009–7 Aug 2010
	3495 m	1911	RCM11	60	31 Jul 2009–5 Sep 2009
		2542	RCM11	60	31 Jul 2009–7 Aug 2010
		3173	ARG	20	31 Jul 2009–22 May 2010
B23-2	47° 05.86′ N				Mooring lost
	43° 07.17′ W				
	3500 m				

[a]Instrument types are WH75: TRDI Instruments 75 kHz WorkHorse ADCP, ARG: Sontek Argonaut, and RCM11: Aanderaa recording current meters with Doppler sensor.

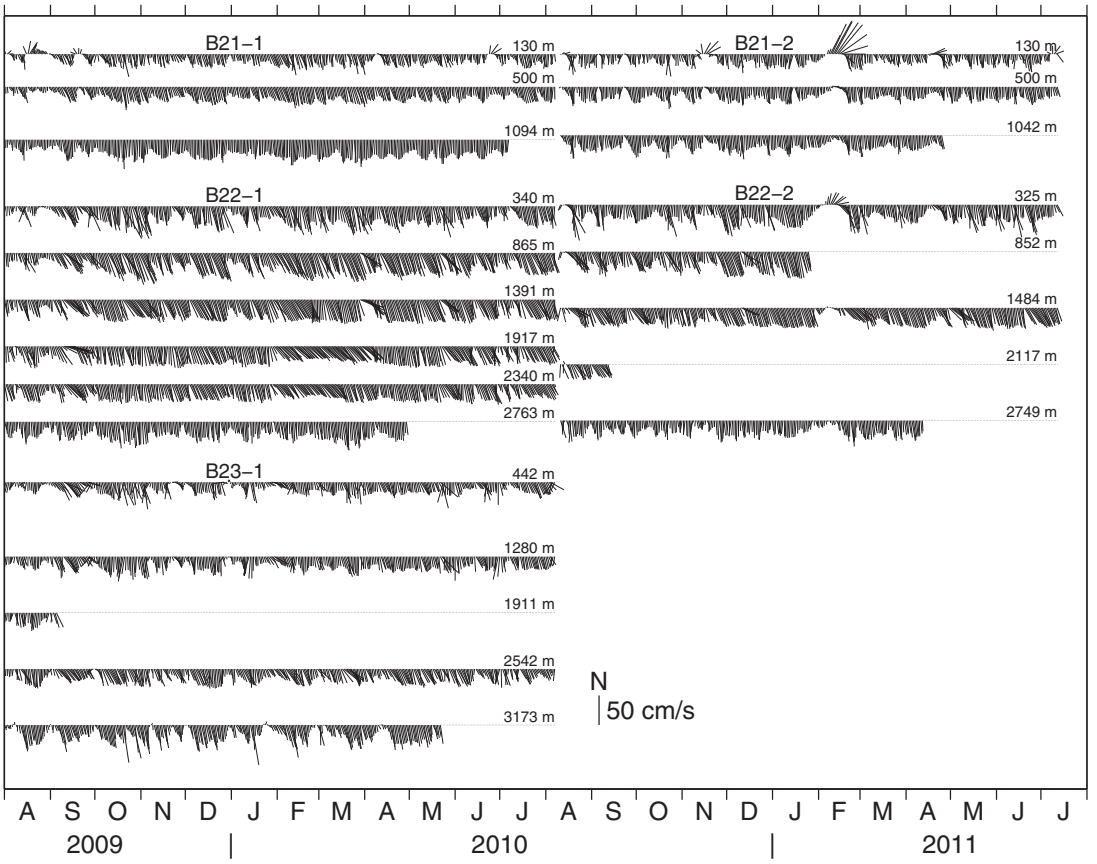

Figure 3. Two year time series of 40 h low-passed current vectors from the Deep Western Boundary Current array for August 2009 to July 2011. Nominal depths are indicated for each time series (cf. Table 2).

missing data. The EOFs were computed from the covariance matrix of the individual time series at the new depths, and the first five modes, explaining 85% of the variability, were then used to reconstruct the missing parts of the time series. The resulting current time series on fixed depths were then used to calculate the transports.

Correlation between individual instruments and the DWBC transport range from 0.4 to 0.95, shown for the first deployment period in Figure 2a. Correlations are highest between 500 and 1000 m depth at the central mooring, while lower correlations are found at instruments below 2000 m at the central mooring and also below 2500 m at the eastern mooring.

To assess a possible offset or errors arising from the handling of the mooring data, the behavior of the moored instruments was simulated and the procedure to fill the gaps was replicated using the VIKING20 model output. The rms difference between the transport calculated from the simulated mooring time series and that calculated using the full grid is 2 Sv. The simulated mooring transports are biased low by 1.7 Sv compared to the full model transport.

2.3. Altimetry

Sea surface height (SSH) above geoid data from 1993 to 2012 are used in the form of delayed-time referenced absolute dynamic topography as provided by AVISO, gridded on a 1/3° Mercator grid with a temporal resolution of 7 days. This absolute dynamic topography is derived from sea level anomalies plus a 7 year (1993–1999) mean dynamic topography based on 4.5 years of GRACE geoid data and in situ measurements from 1993 to 2008.

2.4. VIKING20 Model

The model data to complement the observations come from VIKING20 [*Behrens*, 2013] developed in the framework of the DRAKKAR collaboration [*DRAKKAR Group*, 2007] building on the NEMO ocean model [*Madec*, 2008] and the sea ice model LIM2 [*Fichefet and Maqueda*, 1997]. The model uses an isotropic mesh of $1/20^{\circ}$ longitudinal resolution between 30°N and 85°N (corresponding to a mesh size of less than 4 km in the Newfoundland Basin), embedded in a global model of $1/4^{\circ}$ (ORCA025) via a two-way nesting technique [AGRIF, *Debreu et al*., 2008]. It uses 46 levels in the vertical, starting from 6 m intervals at the surface, smoothly increasing to 250 m at depth. The present simulation is forced with atmospheric fluxes given by the CORE reanalysis product for 1948–2007 [*Large and Yeager*, 2008] after a 30 year spin-up. We used the 5 day average properties for the period from 1960 to 2007.

A model validation against several data sets from the overflow water masses along the DWBC in the subpolar North Atlantic [*Fischer et al*., 2014] found that the model velocities have a maximum spectral variance in the DWBC at intraseasonal periods. The best agreement between model and observations was found for the Flemish Cap/47°N region, where the spectral shape was well reproduced and spectral variance levels were similar or slightly higher than in the observations.

3. Hydrography and Flow Field

The shipboard current measurements along 47°N show several cores of alternating currents in southward and northward direction of varying strength and extent (Figure 4), representing the DWBC, the NAC, and the NBR. The positioning of the cores at this location is closely linked to the shape of the continental margin, which is characterized by the very steep continental slope (44°–43°W), where the seafloor drops from 500 to 3500 m, followed to the east by the gentler slope of the continental rise (43°–41°W), where the water depth increases further to 4500 m. The pattern of alternating flows extends over the entire basin [see *Rhein et al*., 2011, for a full transatlantic section], but toward the east the currents becomes successively weaker and less stationary, giving way to an eddy regime.

At the western boundary, the southward DWBC is divided into two velocity cores. One of the cores is narrow, observed in all realizations, with about 40 km width focused above the continental slope. It has maximum velocities of up to 40 cm s^{-1} in the shipboard observations (Figure 4), typically at intermediate depths around 2000 m. Below 2000 m, the velocity decreases toward the seafloor. The current meter time series show the DWBC core at depths between 1400 and 1800 m with maximum southward velocities of up to 50 cm s^{-1} (Figure 3), and a mean of 30 cm s^{-1} (Figure 2b).

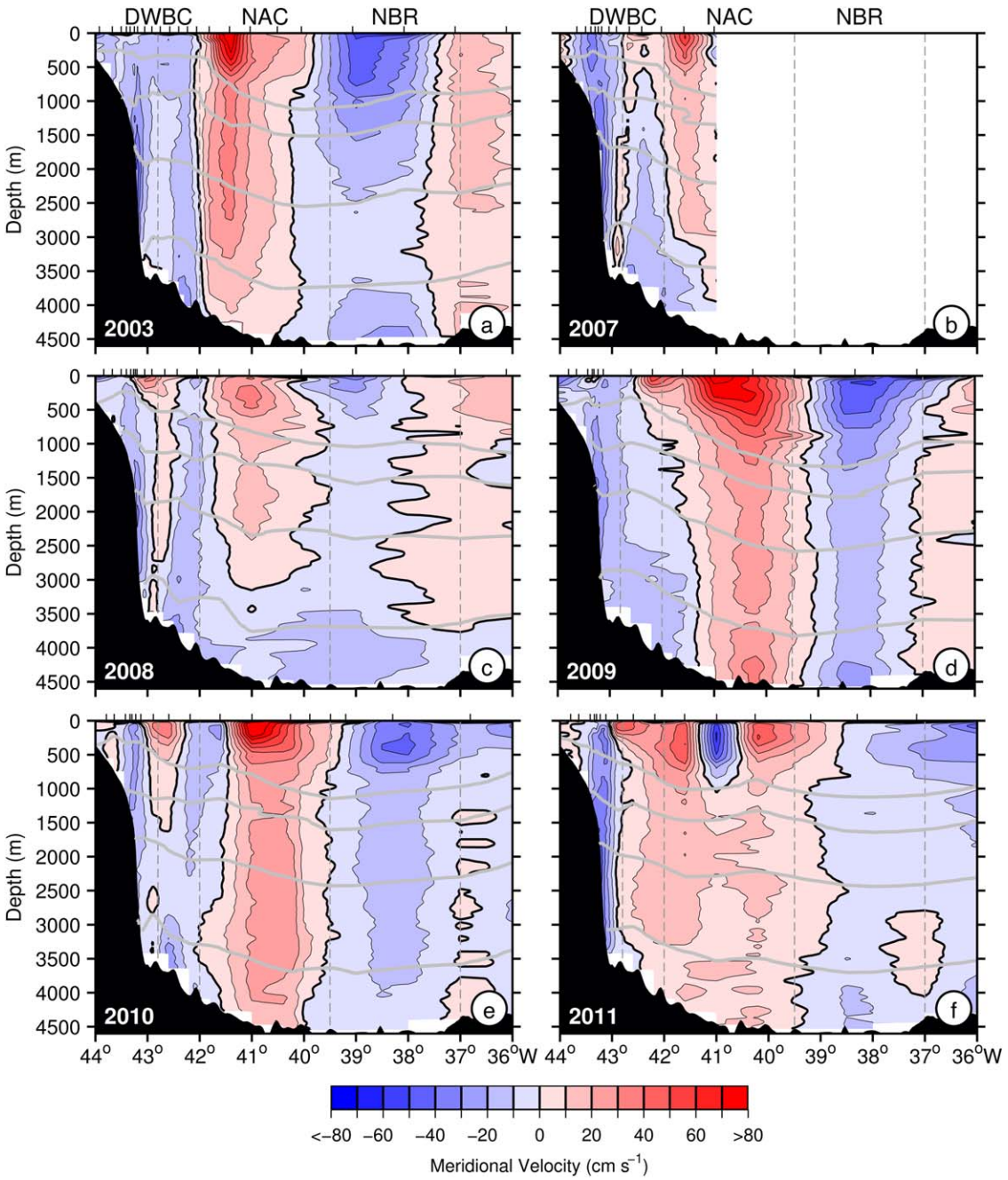

Figure 4. Meridional velocity along 47°N between 44° and 36°W from LADCP measurements carried out on six cruises between 2003 and 2011 (cf. Table 1). Vertical-dashed lines denote the mean longitude bands of the DWBC slope, DWBC rise, NAC, and recirculation. Superimposed are isopycnals used to separate the North Atlantic water masses (σ_θ = 27.68, 27.74, 27.8, 27.88 kg m^{-3}). Stations are indicated at the top of each plot.

The second core of southward flow is found at the continental rise, more variable in shape and strength, and observed in five of the shipboard realizations. In contrast to the first core, the highest velocities of up to 30 cm s^{-1} are found close to the seafloor. These two cores will be referred to as slope DWBC (west of 42.8°W) and rise DWBC core (east of 42.8°W) in the following.

The total southward (northward flow excluded) volume transport of both DWBC cores at the time of observation (Table 3) varies between 25.5 Sv (in 2011, Figure 4f) and 46.3 Sv (in 2009, Figure 4d), with varying proportions of rise and slope current. The slope current is rather stable, and carries a relatively constant deep water fraction ($\sigma_\theta > 27.68$ kg m^{-3}) around 80%, while the rise part is more

Table 3. Total Transports (in Sv) From Shipboard LADCP Measurements and VIKING20 Model Data Across 47°N Section (BC and NBR Southward West of 41°W and Between 37°W and 41°W, respectively, NAC Northward West of 38.5°W); Deep Water Transport Below σ_θ 27.68 kg m^{-3}

	Total Transport				Deep Water Transport			
Year	BC	(Slope/Rise)[a]	NAC	NBR	BC	(Slope/Rise)[a]	NAC	NBR
2003	41.5	(18.1/23.3)	99.5	112.2	36.0	(14.9/21.1)	66.2	62.8
2007	39.8	(20.9/18.9)			35.1	(16.4/18.7)		
2008	38.9	(11.7/27.1)	41.3	54.7	36.2	(10.2/25.9)	20.0	42.3
2009	46.3	(22.4/23.9)	165.1	91.1	40.9	(17.7/23.2)	84.3	44.6
2010	31.8	(10.5/21.4)	125.7	92.5	25.1	(8.8/16.2)	76.8	54.9
2011	25.5	(21.3/4.2)	127.9	37.4	17.5	(17.4/0.1)	79.9	19.2
Mean	37.3	(17.5/19.8)	111.9	77.6	31.8	(14.3/17.5)	65.5	44.8
Std	7.4	(5.2/8.1)	45.8	30.6	8.7	(3.8/9.2)	26.3	16.5
VIKING20								
Mean	60.3	(30.8/29.5)	115.1	57.9	55.1	(29.2/25.9)	68.5	36.2
Std	23.6	(7.9/24.7)	38.4	43.5	20.2	(7.2/20.8)	29.3	23.1

[a]BC slope defined as southward flow west of 42.8°W, BC rise defined as southward flow between 41°W and 42.8°W.

intermittent, and (if present) carries almost entirely dense water due to its bottom intensified nature (Table 3).

The surface intensified NAC with velocities exceeding 1 m s^{-1} is located directly east of the DWBC. The NAC often extends down to the seafloor and is typically strongest between 42° and 39.5°W. East of the NAC between 39.5° and 37°W, a southward current, often of similar strength and lateral extent as the NAC, is found (Figure 4). The eastern boundary of this flow appears to coincide with the base of the Mid-Atlantic Ridge. The total northward volume transport of the NAC across the section (including secondary cores west of 42°W) shows a high variability, with a minimum of 41.3 Sv in 2008 and a maximum of 165.1 Sv in 2009 (Table 3 and Figures 4c and 4d). The northward deep water transport is closely related to the total transport, the ratio between the total transport and the deep water fraction varies between 50 and 66%. In the year of the weakest transport (2008), the northward flow is limited to the uppermost 3000 m, while southward flow is found below (Figure 4c). The southward recirculation east of the NAC shows a similar high variability, with the maximum in 2003 (112.2 Sv, Figure 4a), and the minimum in 2011 (37.4 Sv, Figure 4f), where no clear structure of a southward current core was observed. The percentage of deep water in the recirculation varies between 50 and 75%. The five single realizations show no clear relationship between the strength of the NAC and its recirculation at this latitude.

The deep water masses carried by DWBC and NAC are upper Labrador Sea Water (uLSW), Labrador Sea Water (LSW), Gibbs Fracture Zone Water (GFZW), and Denmark Strait Overflow Water (DSOW). The water mass boundaries for uLSW, LSW, GFZW, and DSOW are marked by the isopycnals $\sigma_\theta = 27.68$, 27.74, 27.80, and 27.88 kg m^{-3}, respectively, following *Stramma et al.* [2004] (Figures 5 and 6). GFZW is also known as Northeast Atlantic Deep Water (NEADW) and originates in the Iceland Scotland Overflow Water (ISOW) [e.g., *Smethie et al.*, 2000].

The horizontal distribution of salinity (Figure 5) is often closely linked to the flow field; the highest salinities in the uLSW and LSW layers are found in the NAC at approximately 40°W, close to the transition between the NAC and the recirculation. In the DWBC, the salinity in the uLSW depth range is lower than in both the NAC and the recirculation (Figure 5). On average, the salinities in the western part of the NAC are lower than in the eastern part, due to the exchange with the boundary current. The gradient between the low salinities at the boundary and the maximum in the NAC band reduces below the LSW. In the DSOW range, the differences between the DWBC and the deep reaching parts of the NAC are negligible, except in close proximity to the topography.

In the recirculation, the salinity in the uLSW and LSW layers is generally lower compared to the NAC (Figure 6), and slightly lower than in the basin interior east of 37°W (not shown). In these layers, the water mass properties of the recirculation represent an admixture of the water carried by the boundary current and by the NAC. The fractions vary from almost entirely boundary current water (2009, Figure 6d) to dominantly water from the NAC (2003 and 2010, Figures 6a and 6e). The highly variable and often lower salinity of the NBR compared to the NAC indicates a variable cross-frontal lateral exchange between these currents north

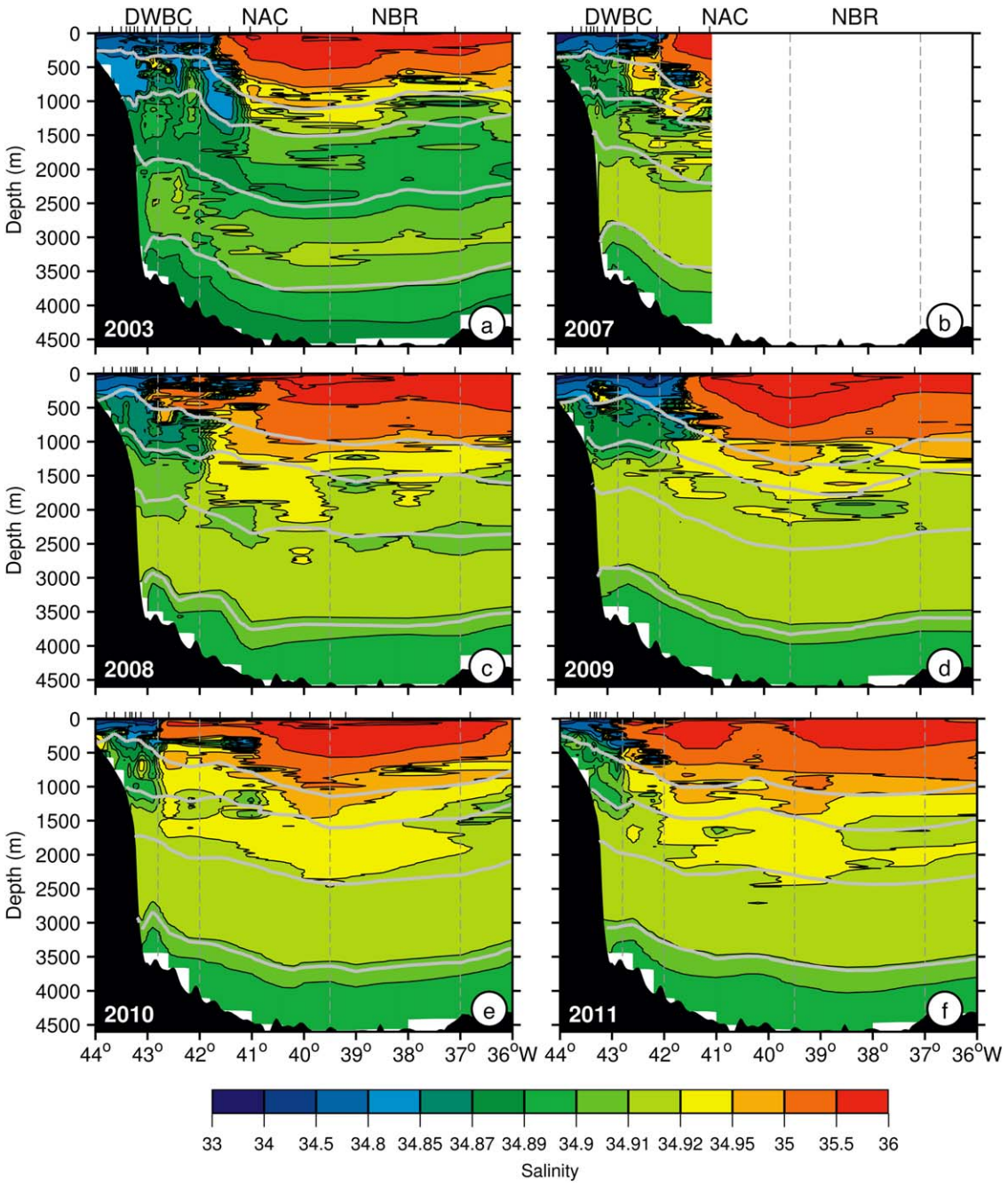

Figure 5. As Figure 4, but for salinity.

of 47° N in the Newfoundland Basin. Between 2003 and 2007 (Figures 5a and 5b), the GFZW has become more homogeneous, indicating changes in the formation history of this water mass body.

3.1. Synoptic Variability

The main current system in the Newfoundland Basin is strongly influenced by mesoscale variability. In 2008 and 2010, deep reaching cyclones of about 50 km diameter were wedged between the NAC and the DWBC (Figures 4c and 4e), altering the rise core of the DWBC and resulting in the two lowest transports of all realizations in the slope core of less than 10 Sv of deep water (Table 3). Of these two situations, the 2010 eddy has a clear surface signature with the minimum in SSH near 42° W north of the section (Figure 7e). Both of

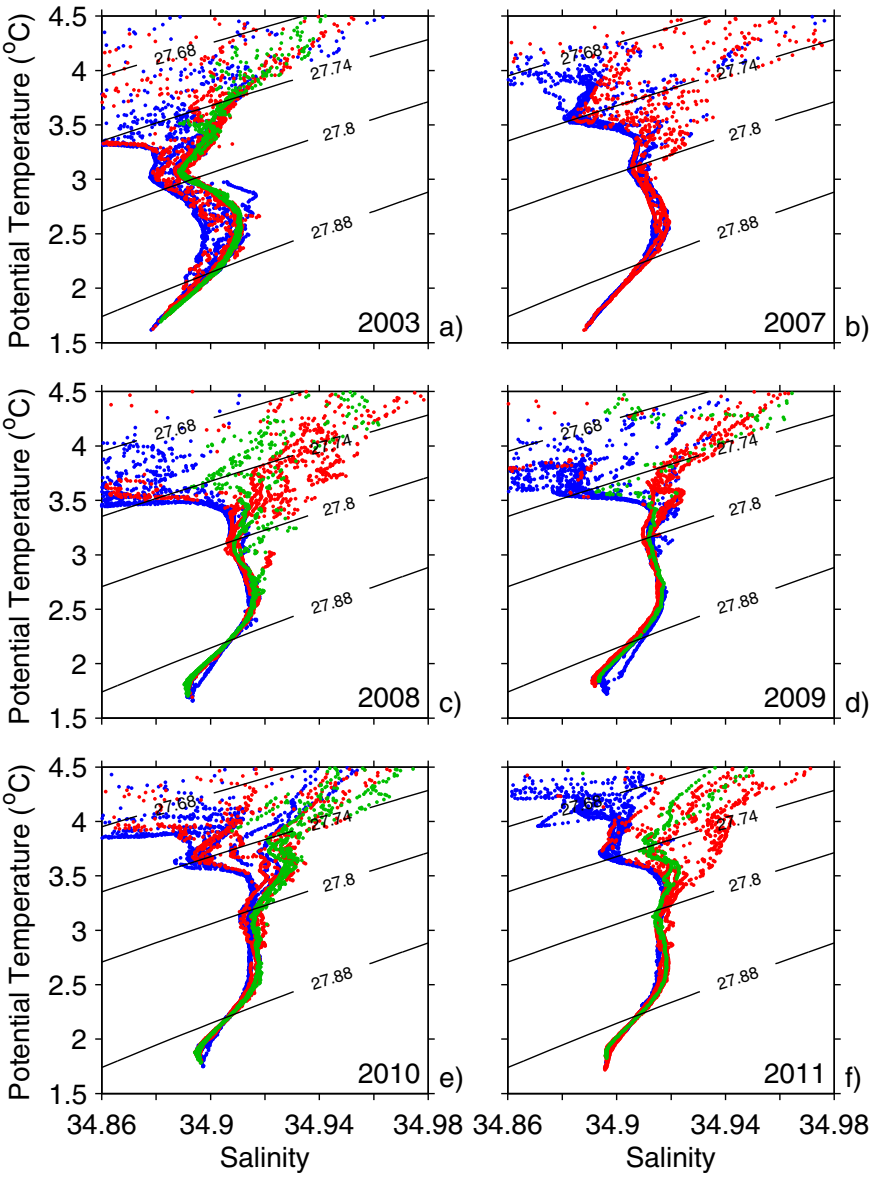

Figure 6. Temperature-salinity diagrams from CTD casts along 47°N between 44° and 36°W from years 2003 to 2011 color-coded by flow direction: Northward flow (NAC, red), southward flow west of 41°W (DWBC, blue), southward flow east of 41°W (NBR, green). Added are isopycnals $\sigma_\theta = 27.68, 27.74, 27.8, 27.88$ kg m^{-3} separating uLSW, LSW, GFZW, and DSOW, respectively.

these eddies carry lenses of low salinity uLSW and LSW away from the boundary into the NAC as well as high salinity water towards the boundary at the surface (Figures 5c and 5e). In 2009 the secondary maximum of northward flow at 42°W (inshore of the NAC; Figure 4d) corresponds to a cyclone north of the section (Figure 7d) carrying very low salinity water at the surface (Figure 5d). In 2011, the NAC is broad, completely replacing the rise core of the DWBC (Figure 4f). A shallow cyclone confined to the upper 1000 m is embedded in the NAC, centered approximately at 40°30′W (Figure 7f). Possible traces of undiluted GFZW are occasionally observed in the deep water in the form of lenses of warmer, more saline water, in the core of the NAC (e.g., in 2008; Figures 5c and 6c), and also the boundary current (2003, 2009; Figures 5a, 6a, and 6d).

The properties of the water masses along 47°N show a considerable amount of long-term variability with an increase of salinity and temperature with time as the general trend (cf. Figure 6). To separate the spatial variability connected to the flow field from this long-term trend, salinities on isopycnal surfaces along the 47°N

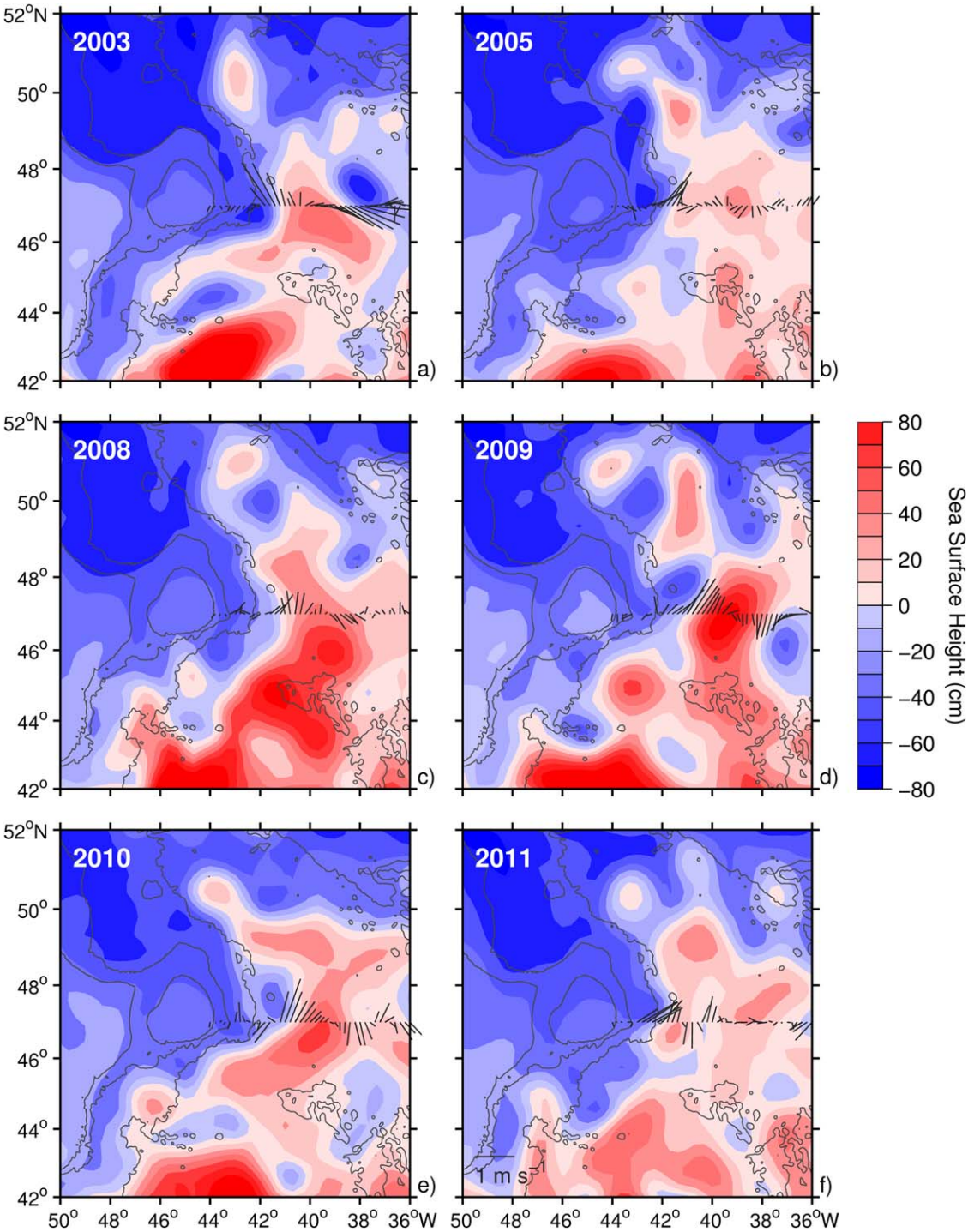

Figure 7. Absolute dynamic topography gridded on 1/3° from AVISO and mean velocity in the upper 100 m along 47°N from shipboard ADCP data.

section are shown in Figure 8. It can be seen that while the salinities are still generally increasing in the overflow water masses, the trend has come to a halt in the uLSW/LSW layer, where the horizontal variability is dominant.

The largest horizontal gradients in the water mass properties are found in the uLSW layer (Figure 8a). In the range between 41° and 43°W, two different regimes were observed. In some realizations (2007, 2010, 2011), there are relatively high salinities found, indicating a strong admixture of NAC water. On the other hand, during 2003, 2008, and 2009 minima in salinity were observed that show the signature of water from the

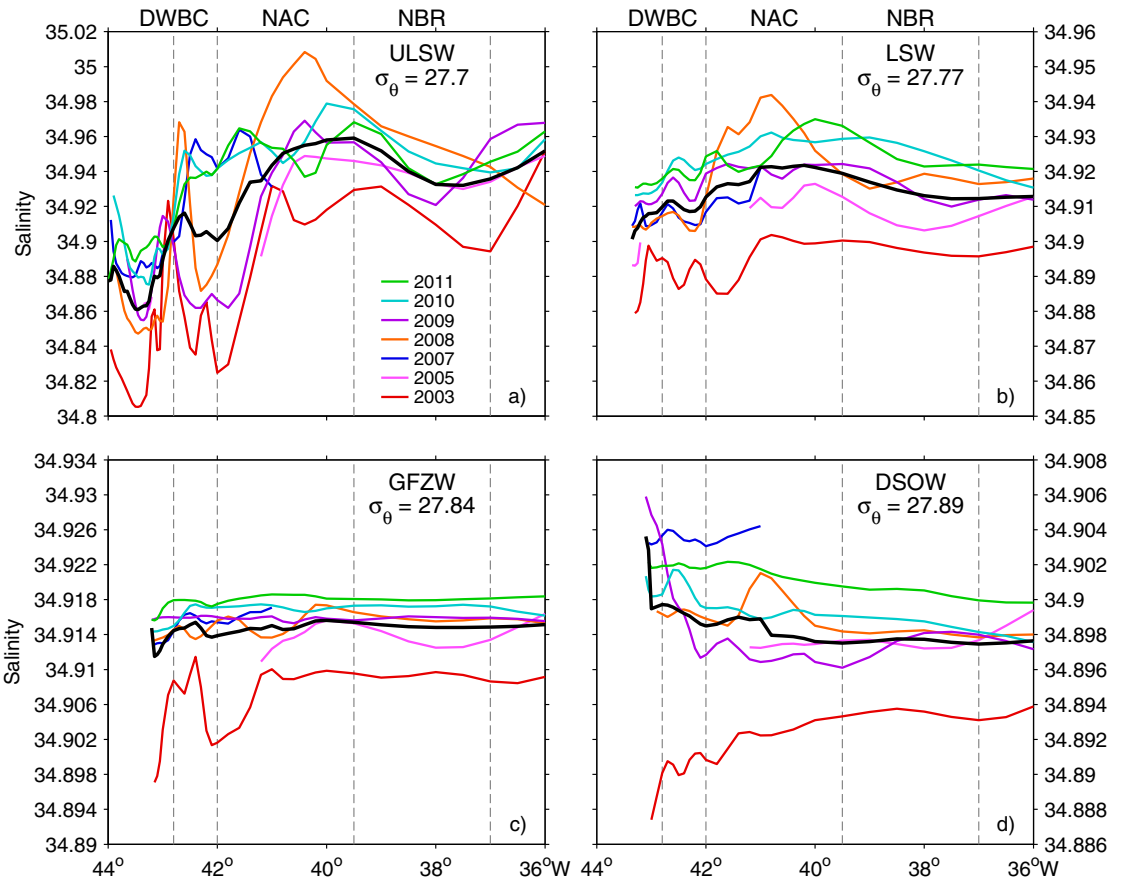

Figure 8. Salinity on density surfaces representing uLSW (a), LSW (b), GFZW (c), and DSOW (d) from all CTD data along 47°N from years 2003 to 2011. The thick black line is the average of all years, vertical-dashed lines denote the longitude bands of the DWBC slope, DWBC rise, NAC, and recirculation.

boundary current propagating offshore upstream of 47°N (cf. Figures 5a, 5c, and 5d). Over the slope part of the boundary current, there is little or no evidence of interaction with the NAC in the uLSW layer.

With few exceptions, the variability within water masses east of 41°W in the LSW and GFZW layers is small (Figures 8b and 8c), and there are little horizontal gradients between NAC and NBR, especially in the GFZW. The absence of the formation of new LSW in recent years has lead to an equalization of the salinity between the boundary current and the interior. The higher year-to-year and along-section variability of the DSOW (Figure 8d) compared to the GFZW reflects its short-spreading time from the source region [*Stramma et al.*, 2004]. There is also little difference between the salinity of the NAC and the recirculation in the GFZW and DSOW layers, except in the GFZW in 2005 (Figure 8c) and the DSOW in 2008 (Figure 8d). Although the transport across 47°N is low in 2008, the high salinities in the NAC in all layers (top-bottom) (Figure 8), as well as the large scale structure of sea surface height (Figure 7c) indicate a continuous advection of high salinity waters from the south toward this latitude.

3.2. Time-Averaged Transport

The short-term variability between the individual realizations is high, but a comparison between the observed mean flow structure with the output of the high-resolution VIKING20 model and satellite altimetry time series indicates that the average fields from the shipboard observations are remarkably representative of the mean state from 47 years of model output as well as from 19 years of altimetry from AVISO (Figure 9). The structure of the mean meridional velocity in the observations shows clearly the two cores of the boundary current, as well as the NAC and its recirculation in the observations (Figure 10a). This average structure of the current system at 47°N is well reproduced in the VIKING20 model (Figure 10b).

Five of the seven cruises give a full coverage of the NAC and its recirculation (Table 1). The total mean northward NAC transport from this five realizations is 111.9 ±20.5 Sv, thereof 65.5 ±11.7 Sv in the deep

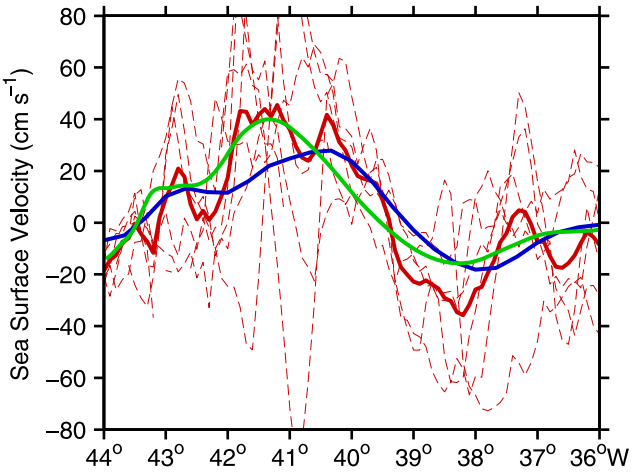

Figure 9. Meridional surface velocity at 47° N from shipboard ADCP (dashed red: individual realizations; solid red: average from all cruises) compared to long-term averages from AVISO altimetry (years 1992–2012, blue), and VIKING20 model (years 1960–2007, green).

water below $\sigma_\theta = 27.68$ kg m^{-3} (Table 3). The southward recirculation amounts to 77.6 ±13.7 Sv, with 44.8 ±7.4 Sv of deep water. The indicated confidence limits of the mean estimated from the standard deviations given in Table 3 are thus around 20% for the NAC and the recirculation. The total transports in the VIKING20 model are remarkably similar, with a mean of 115.1 Sv total northward transport for the NAC, and 57.9 Sv for the southward recirculation over the 47 year model run (cf. Table 3).

The boundary current was covered by six ship sections (Table 1). The measurements result in a total southward transport below the density surface $\sigma_\theta = 27.68$ kg m^{-3} of 31.8 ±3.6 Sv, with 14.3 ±1.6 Sv in the slope core, and 17.5 ±3.8 Sv contributed by the rise core (Table 3). The southward deep water transport below 400 m derived from the mooring array at the continental slope ranges typically from 5 to 25 Sv (Figure 11). The mean transport from the 2 year time series is 16.3 Sv with a standard deviation of 4.0 Sv. The net transport was generally southward during the 2 years of deployment, interrupted by 2 weeks of northward flow in February 2011, during which a maximum northward transport of 14.6 Sv was observed (cf. Figure 3). The northward flow is the result of a westward meandering of the NAC, an irregular but not totally uncommon occurrence that blocks the DWBC for the time of its duration. The LADCP transport estimates for the DWBC slope core from the deployment and recovery cruises cannot be compared directly with the measurements from the current meter array as they fall into the gaps between the transport time series. However, they correspond well with the measurements from the mooring array shortly before and after (Figure 11). In the VIKING20 model, the total southward deep water transport is 23.5 Sv higher than the combined DWBC deep water transport from the shipboard observations (Table 3). The two cores of the DWBC in the model have mean transports of 29.2 Sv above the continental slope and 25.9 Sv above the rise, respectively.

4. Intraseasonal to Interannual Variability

The observed mean state is superimposed by temporal variability; although the observed transport from the mooring array shows no apparent seasonal cycle, there is a large variability on shorter time scales (Figure 11).

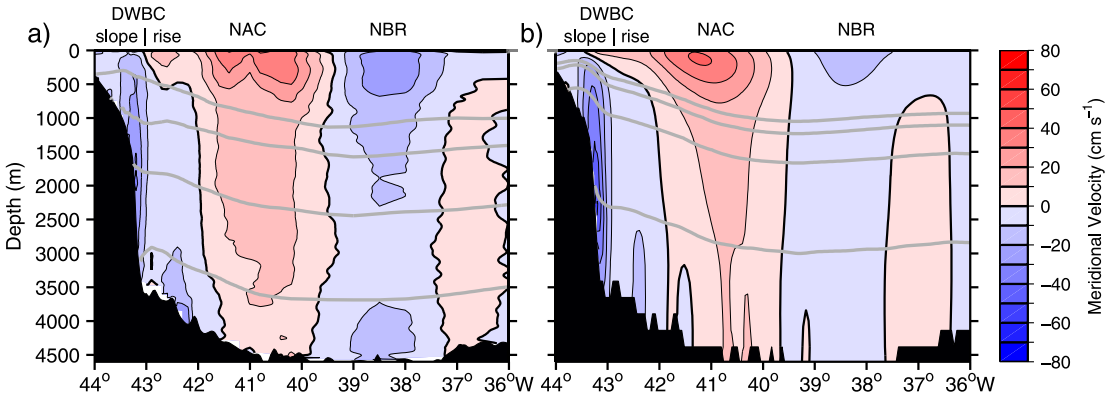

Figure 10. (a) Mean meridional velocity at 47° N between 44° and 36° W from LADCP measurements carried out on six different cruises. Superimposed are isopycnals $\sigma_\theta = 27.68$, 27.74, 27.8, 27.88 kg m^{-3}. (b) 47 year mean of meridional velocity along 47° N from VIKING20 model data.

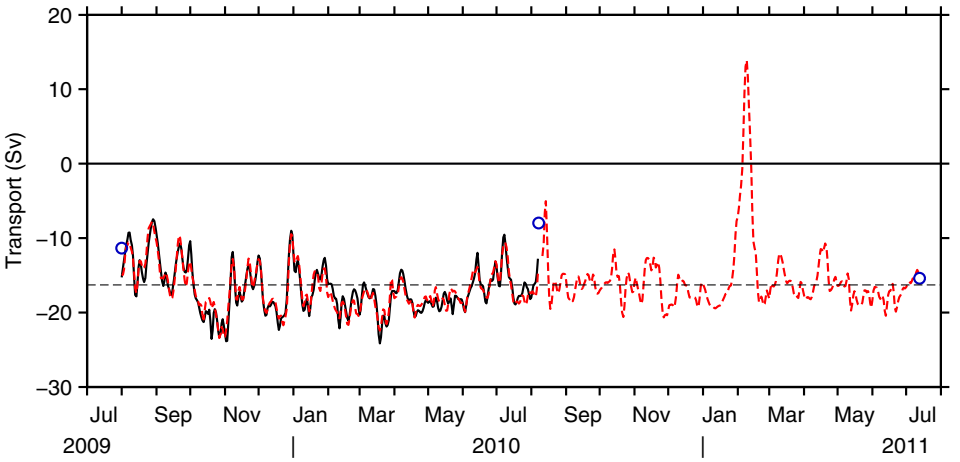

Figure 11. Time series of the net deep water transport of the boundary current above the continental slope below $\sigma_\theta = 27.68$ kg m^{-3} (corresponding to ≈ 340–400 m depth). Shown are the 3 day low-pass-filtered transport using all current meters (black), the reconstruction and continuation using one current meter from the central mooring that shows the highest correlation with the transport (red), and the LADCP estimates from the ship surveys (blue circles, cf. Table 3). The mean transport from the 2 year current meter times series is shown as dashed line.

The agreement of mean velocities and structures along 47°N found between model, satellite altimetry, and direct observations supports the use of the model output and the AVISO data to study long-term variability.

4.1. Intraseasonal Current Variability

Variance preserving spectra of the meridional velocity calculated from 128 day half-overlapping segments show in general a maximum of variability at time scales between 20 and 50 days (Figure 12). At the shallowest mooring (B21), the spectra show little variation with depth, whereas at the central mooring (B22) the two uppermost records have maximum values, followed by a minimum of variability at mid-depth in the core of the DWBC. The 40 day spectral peak in the two topmost records of B22 is amplified by the current reversal in February 2011 that was strongest for these instruments (cf. Figure 3). Time series of surface geostrophic velocity from satellite observations (Figure 13) show that a current reversal at the surface close to the western boundary (as during the February 2011 event) is not uncommon. However, from the several occurrences during 2010/2011, only this one was deep reaching and therefore influencing the mooring record. A secondary maximum of variability is found at periods of less than 10 days. At the eastern mooring (B23), the structure is similar to the central mooring, except for the lowermost instrument that shows the highest variance of all records, albeit with maxima in the same frequency bands.

The zonal velocity component is generally less energetic, with almost no variability close to the seafloor; here, fluctuations are suppressed by the proximity of the lateral boundary. The variability occurs in the same frequency bands as the variability of the meridional components. At mooring B22, the variability on timescales between 20 and 50 days has its maximum at mid-depth, where the fluctuations in the meridional component were at minimum. There is a pronounced peak for the periods below 10 days that have their maximum in the two uppermost current meter records.

The variability at less than 10 days periods is likely the signature of coastal trapped Rossby waves (CTWs) which likewise have been observed farther upstream at 53°N [*Fischer et al.*, 2014]. The similar modal structure in the meridional and zonal components at B22 indicates variations of the direction of flow at the mooring location that exert the biggest effect on the zonal component at the depth of the maximum flow speed. The 20–50 day periodicity translates to a length scale of 25 to 65 km—approximately the boundary current width—for a wave speed of 1.5 cm s^{-1}, the typical propagation speed of baroclinic Rossby waves at this latitude [e.g., *Chelton et al.*, 2007] and can be interpreted as incoming waves or eddies from the east. In the satellite observations (Figure 13), the strength of the currents decreases rapidly east of the recirculation at about 37°W and gives way to a predominantly wave dominated regime. Incoming signals from the east take approximately 1 year to propagate from 30° to 36°W, again corresponding to a westward velocity of

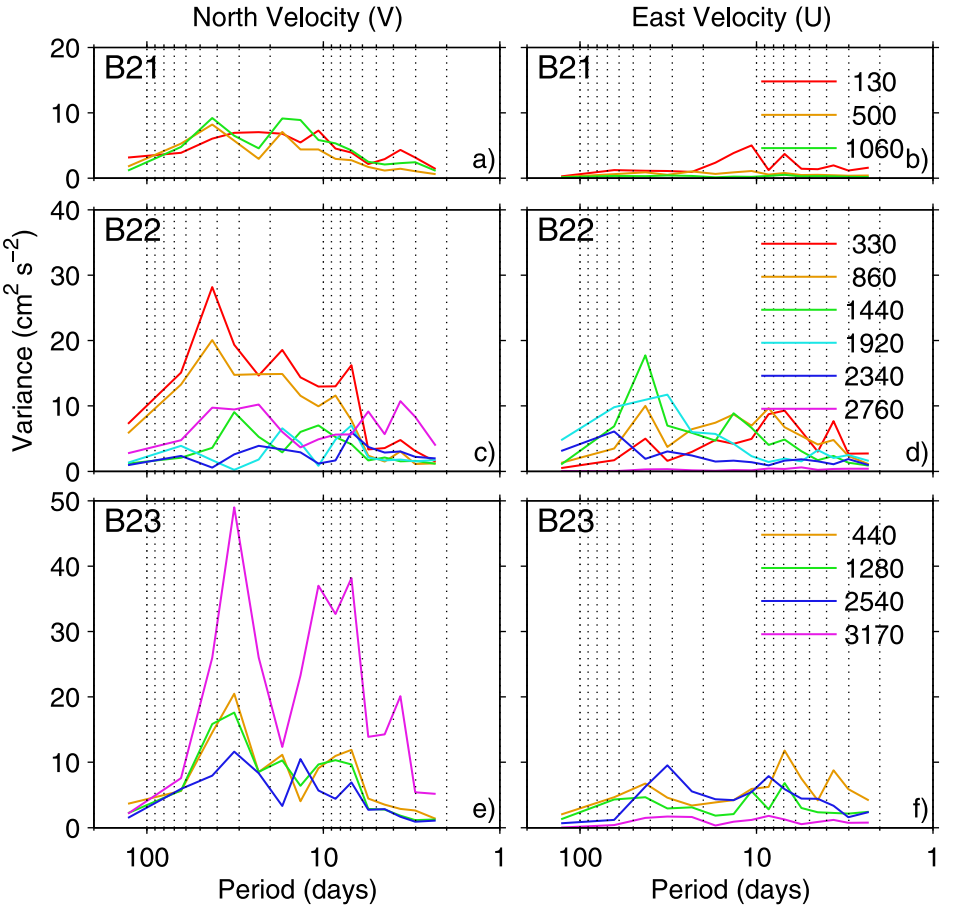

Figure 12. Variance-preserving spectra from 128 day half-overlapping segments of meridional (v, left) and zonal velocity (u, right) fluctuations at the Deep Western Boundary Current moorings. Two year long-time series are used at mooring B21 (a, b), and where available B22 (c, d), and 1 year long-time series at B23 (e, f). The approximate nominal instrument depths (m) are given in the legends.

1.5 cm s^{-1}. Periods of pronounced wave signals in the interior (e.g., in 2005) often coincide with periods of weak recirculation signals in the NAC/NBR regime.

4.2. Coherence of NAC and Recirculation

The model time series of meridional transport at 47°N shows energetic short-term fluctuations (Figures 14 and 15); however, a low-pass filtered time series also exhibits considerable variability on the intraseasonal to interannual time scales, except for the DWBC slope core that is relatively stable and shows little long-term variability (Figure 14a). Interannual variability of the boundary current in the model finds its expression mainly in the rise core (Figure 14b) whose variations are in remarkable agreement with the other two major components of the flow field, the NAC and its recirculation (Figure 15). In the shipboard observations, the standard deviation of the transport estimate of the slope core is more than 50% smaller compared to that of the rise core, which is an indication of a similar behavior as in the model, with a more stable current core above the slope.

Variance-preserving spectra of model velocity times series have been calculated at fixed locations along 47°N in the cores of the NAC and the two parts of the DWBC. They all show an increasing variance on short-times scales from 10 to 40 days (Figure 16a). For periods longer than 40 days, the variance in the two DWBC cores decreases, while it rises further in the NAC and then drops on time scales beyond 100 days. Correlations found between the individual model velocities depend on the considered periods of variability (Figure 16b). On the shorter times scales between 20 and 40 days, a squared coherency between 0.2 and 0.4 is found for the two boundary current cores as well as for the NAC and the DWBC rise core. Little squared coherency of 0.2 at maximum for periods near 30 days is found between the times series in the NAC the DWBC rise core. The squared coherency between the velocities in the two boundary current cores drops on longer time scales and vanishes for periods

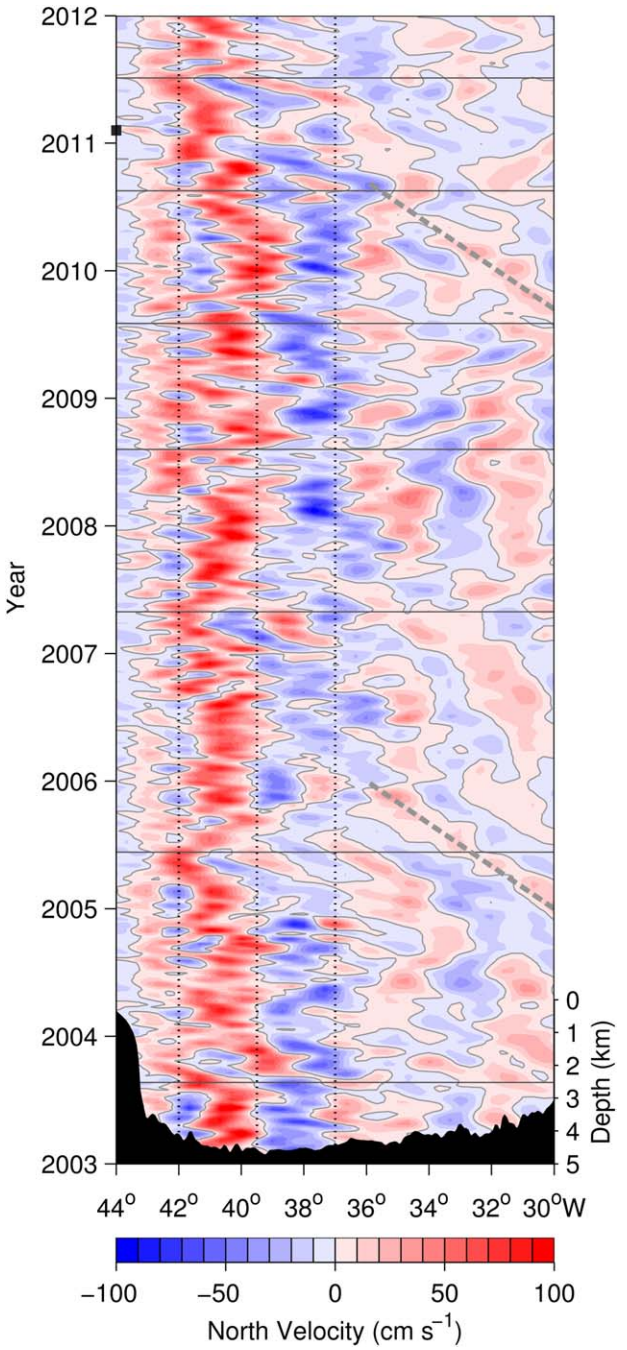

Figure 13. Hovmöller diagram of surface geostrophic velocity along 47°N from absolute altimetry (AVISO), with bathymetry (ETOPO2) superimposed at the bottom of the figure. Gray lines mark the dates of the hydrographic surveys, black-dotted lines denote the horizontal range of the NAC and its recirculation as used in the text, black square on the *y* axis marks the time of current reversal in mooring record. Stippled in grey indicate typical Rossby wave speed of 1.5 cm s^{-1} for purpose of comparison.

longer than 100 days. In contrast, the squared coherency between NAC and DWBC rise core increases for longer time scales and reaches its maximum values of about 0.6 for periods between 300 to 400 days.

The total correlation between the NAC and the recirculation on timescales longer than 100 days is high (0.78 for the 100 day low-pass filtered time series, Figure 15). This correlation increases further if the southward transport of the DWBC rise core is included in the recirculation (0.90 for 100 day low-pass). On the other hand, the variability of the DWBC slope core shows no correlation (0.08) with the NAC and an inclusion does not heighten the correlation between the recirculation system and the NAC. Thus, an increase in the NAC strength is (in the model) largely compensated by the recirculation, but also by a strengthening of the DWBC rise core. There is no lag in this response of the NAC/NBR/BC rise system, the model fluctuations adjust quasi instantaneous on synoptic timescales of a few days. The concurrent changes of the NAC and the rise core of the DWBC in the model indicate a simultaneous response of both in reaction to changes in the forcing. The partitioning of the southward transport changes in the DWBC rise core and the NBR in conjunction with the NAC fluctuations is on average almost equal. However, the increase in correlation with the NAC transport for the combined transport of both DWBC rise core and NBR indicates temporal fluctuations in this partitioning (Figure 15). By contrast, the DWBC slope core is decoupled from the NAC variability. The mean transport residual between the NAC and the NBR/DWBC system that has to recirculate east of 37°W is small, 3.1 Sv with a standard deviation of 23.4 Sv for the fully resolved time series and 12 Sv for the 100-day low-pass filtered data.

4.3. Interannual Variability

In the surface geostrophic velocity derived from SSH observations (Figure 13), the short-term variability of the circulation at the surface is also modulated by extended periods of either higher or lower southward

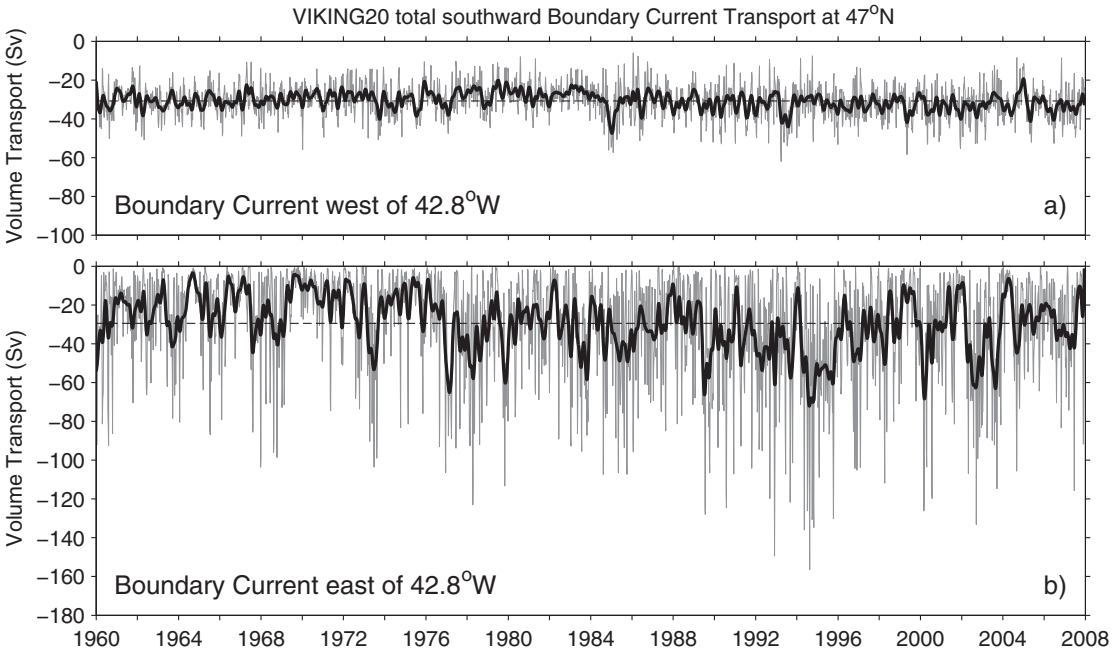

Figure 14. Time series of top-to-bottom boundary current transports every five days (gray) and 100 day low-pass filtered (black) in the VIKING20 model. (a) Above the continental slope west of 42.8° W and (b) above the continental rise between 42.8° and 41° W. Mean transports are shown as dashed lines.

velocities in the NBR in the time series. Stronger recirculation signals are observed from 2003 to 2005 and between 2008 and the end of 2010, while weaker currents dominate from 2005 to 2008 and after 2010. Notably, similar patterns of strong and weak recirculation periods can be seen in the model (Figure 15), e.g., the period from 2003 to 2004, during which the transport in NAC and recirculation is also higher than average in the model. On interdecadal time scales, the model results show a long period of strong recirculation (NBR + DWBC rise) from the mid 1980s to the mid 1990s with a total southward transport generally exceeding 120 Sv, followed by a weakening in the late 1990s. Periods of weak recirculation are also evident in the 1960s and 1970s, most notably between 1969 and 1972.

5. Circulation in the Newfoundland Basin

In spite of the large amplitude of the temporal variability, a mean pattern of circulation in the Newfoundland Basin can be deduced from the present observations and is schematically summarized in Figure 17. On average, the largest volume transport across 47° N of 111.9 Sv is carried by the northward NAC (Table 3). Two thirds of the northward flow are compensated by a southward recirculation east of the NAC, resulting in a net northward transport of 34.3±17.4.0 Sv that is composed of 20.7 ±9.8 Sv deep water and 13.6 ±8.8 Sv in the surface layer. This residual flow continues northward toward the Northwest Corner where a top-to-bottom transport of 50 Sv was derived from current meter measurements by *Lazier* [1994]. The excess transport is likely part of a northern recirculation cell that is evident in altimetry (Figure 7) as well as float and drifter trajectories [*Lazier*, 1994; *Bower et al*., 2002; *Reverdin et al*., 2003]. After turning east, when the NAC crosses the Mid-Atlantic Ridge, the average total transport from the years 2006 to 2010 is 29.4 Sv, with 11.5 Sv of deep water [*Roessler*, 2013, geostrophic transport from inverted echo sounders]. This constitutes the major part of the NAC in the Northwest Corner, while the remaining fraction supplies the recirculation of 6 to 15 Sv observed in the Labrador Sea [*Fischer et al*., 2004, 2010]. The difference between the northward NAC transport and the southward transport in the NBR in the surface layer is less than the surface transport across the Mid-Atlantic Ridge of 17.9 Sv [*Roessler*, 2013], leaving an imbalance of 4.3 Sv, which is below the error limits of the transport estimates.

In the VIKING20 model, the mass budget across 47° N is somewhat different from the observations (cf. Table 3). While the total NAC transport is similar both for the total and in the deep water, the recirculation in the

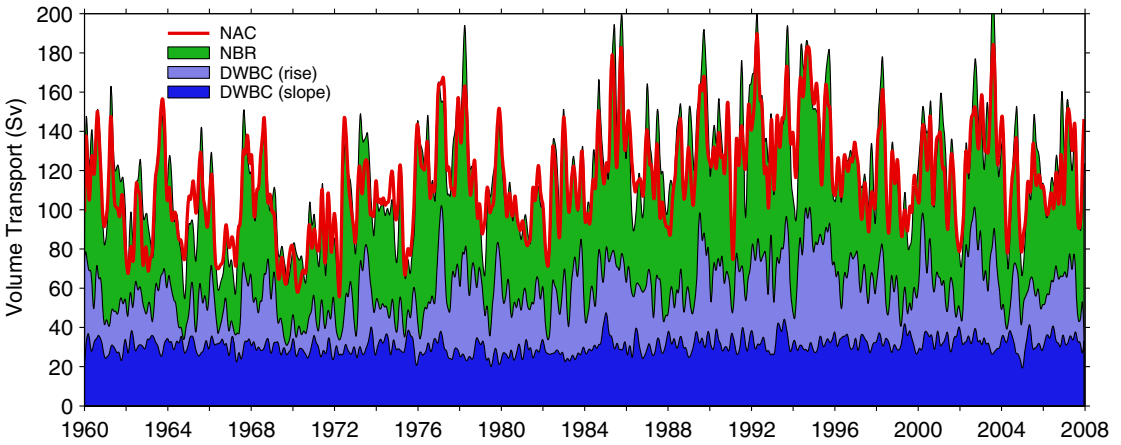

Figure 15. Accumulated top-to-bottom southward volume transport across 47°N partitioned by the contributions of the boundary current above the slope (dark blue), the boundary current above the rise (light blue), and the recirculation in the Newfoundland Basin (NBR) between of 41° and 37°W (green). The accumulated southward transport is mostly in balance with the northward transport of the NAC, shown in red.

NBR is weaker by about 20 Sv, which instead appear to return in the boundary current. This would require a recirculation of 35 Sv from the boundary current into the NAC south of 47°N, and result in an overturning circulation of 20 Sv.

The net northward transport at 47°N has to be supplied by both import from the subtropical gyre in the NAC and a recirculation of subpolar gyre water from the boundary current. Observations of the northward NAC transport are available from hydrographic, current meter, and inverted echo sounder measurements southeast of the Grand Banks near 42°N along WOCE line A2/AR19. *Schott et al.* [2004] found a northward NAC transport of 141.6 Sv (60.4 Sv within the deep water layer below $\sigma_\theta = 27.68$ kg m^{-3}) which is close to the 146 Sv estimated by *Meinen and Watts* [2000]. However, at this location, a large amount of the transport recirculates east of the NAC within the so-called Mann Eddy [*Mann*, 1967]. *Lumpkin et al.* [2008] calculated NAC transports of 100–150 Sv and a recirculation of 75–100 Sv within the Mann Eddy from inverse modeling (*Lumpkin et al.*, 2008, Figure 8).

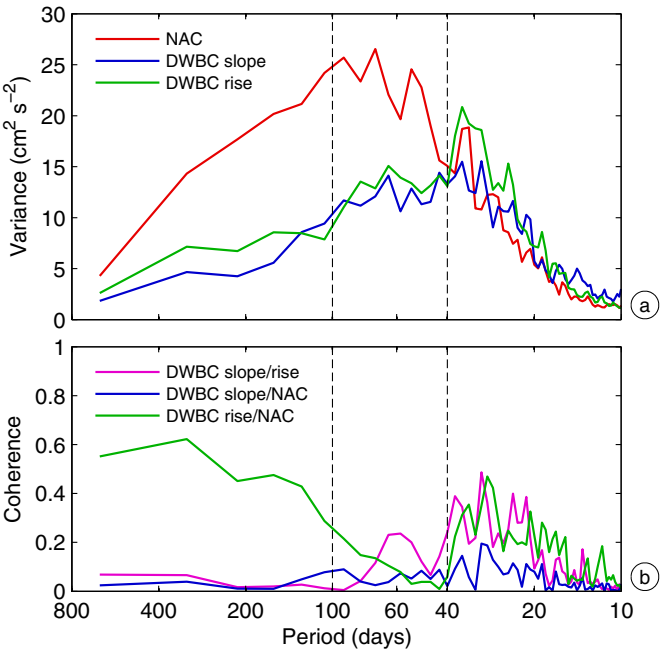

Figure 16. Variance preserving (a) and coherence (b) spectra from 640 day (128 points) half-overlapping segments of current speed from VIKING20 model at fixed locations along 47°N, corresponding to the respective maximum velocities in the mean field (cf. Figure 10b) at a depth of 2000 m (DWBC slope, NAC) or 3200 m (DWBC rise). Dashed lines denote spectral gap between low (periods < 100 d) and high frequency (periods < 40 d) squared coherency of the DWBC rise and the NAC. Note that variability on shorter timescales (< 20 d) is not well-resolved because of the 5 day resolution of the time series in the model.

Schmitz and McCartney [1993] give transport estimates for the NAC system in the Newfoundland Basin with a total transport of 86 Sv for the NAC (49 Sv is deep water below 7°C), and 61 Sv for the recirculation (36 Sv deep water), resulting in a net transport of 25 Sv (13 Sv deep water) across the Mid-Atlantic Ridge. The choice of the 7°C isotherm as the boundary

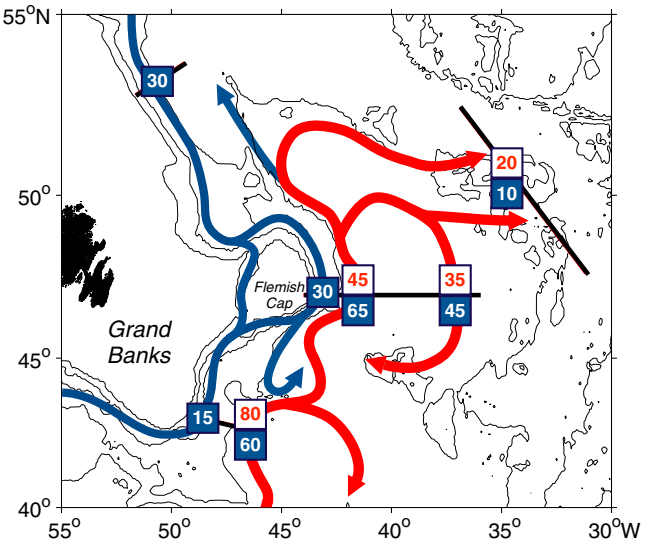

Figure 17. Circulation and transports summary; red boxes: warm water transports above $\sigma_\theta = 27.68$ kg m^{-3}, blue boxes: deep water transports below 27.68 kg m^{-3}; numbers in Sv (rounded to multiples of five; see text for details). Additional transport data from boundary current at 53°N from *Fischer et al*. [2004, 2010]; *Dengler et al*. [2006]; boundary current at 42°N from *Schott et al*. [2004, 2006]; NAC at the Mid-Atlantic Ridge from *Roessler* [2013]. NAC/NBR transports are derived from repeated LADCP sections, other transports from multiyear moored arrays.

between deep and surface water is shallower than the isopycnal $\sigma_\theta = 27.68$ kg m^{-3} used in the present work (which corresponds to temperatures between 4 and 4.5°C for salinities around 34.9), therefore the distribution between surface and deep water transports is shifted toward higher transports in the deep water. Nevertheless, the numbers for the combined transports of the system are considerably smaller than those inferred here; while the surface water transports are at least of a comparable magnitude, the deep water transport is lower by 30% compared to the present observations. However, the ratio between northward NAC transport and recirculation is similar, with more than 2/3 of the water recirculating.

The total southward boundary current transport at 47°N east of Flemish Cap from the shipboard observations amounts to 37.3 ±3.0 Sv, 31.8 ±3.6 Sv thereof in the deep water layer (Table 3). This is close to the observations of *Fischer et al*. [2010] at 53°N, who estimated 41.8 Sv from 9 LADCP sections (Table 4); time series measurements from a mooring array at that location resulted in a slightly lower estimate of 37.2 Sv [*Fischer et al*., 2004] which however corresponded to earlier LADCP estimates from *Fischer et al*. [2004] and *Dengler et al*. [2006]. Farther north at 56°N a lower boundary current transport of 35.0 Sv was observed [*Dengler et al*., 2006]. *Xu et al*. [2013] found a boundary current transport of 39.0 Sv at 53°N based on a 37 year HYCOM simulation. Further they observed a decrease from a period of high transport (1984–1997) to a period of low transport (1997–2010) by 4 Sv, which is about 10% of the total transport. Offshore of the boundary current a recirculation is found in the Labrador Sea that reduces the net transport. The observed recirculation strength at 53°N varies between 5.6 Sv and 15 Sv [*Dengler et al*., 2006; *Fischer et al*., 2004]; at 56°N *Dengler et al*. [2006] found a recirculation of 9.3 Sv.

Despite its high intraseasonal variability, the boundary current appears to be relatively stable and continuous along the continental margin between 56°N and 47°N; further south at 42°N, the transport is reduced to the part which forms the DWBC slope core at 47°N. The flow of uLSW through the Flemish Pass east of

Table 4. DWBC Transport Estimates at Different Latitudes From North to South Along the Western Boundary; Top-to-Bottom and Deep Water Below $\sigma_\theta > 27.68$ kg m^{-3}[a]

Source	Period	Method	Top-to-Bottom	Deep Water (Slope)
Dengler et al. [2006], 56°N	1996–2005	LADCP	35.0 Sv	28.7 Sv
Fischer et al. [2004], 53°N	1996–2001	LADCP	37.7 Sv	25.4 Sv
	1997–1999	Moorings	37.2 Sv	25.2 Sv
Dengler et al. [2006], 53°N	1996–2005	LADCP	37.3 Sv	31.0 Sv
Fischer et al. [2010], 53°N	1996–2007	LADCP	41.8 Sv	35.5 Sv
Xu et al. [2013], 53°N	1978–2011	HYCOM	39.0 Sv	34.5 Sv
This study, 47°N	2003–2011	LADCP	37.3 Sv	31.8 Sv (14.3 Sv)
	2009–2011	Moorings		(16.3 Sv)
Schott et al. [2004] 42°N	1993–1995, 1999–2001	Moorings		12.9 Sv
Schott et al. [2006] 42°N	1999–2005	LADCP	22.7 Sv	17.5 Sv

[a]The transport numbers at 53°N and 56°N give the boundary current transport minus the recirculation in the Labrador Sea (see text for details).

Flemish Cap contributes to the total southward deep water transport, but is below the error limit for our DWBC transport estimate, and not explicitly considered here. Thus, at 47°N, the observations show a boundary current that is basically the same as further upstream in the Labrador Sea, indicating the deep reaching subpolar gyre extends across 47°N at the western boundary.

South of Flemish Cap at 42°N, *Schott et al*. [2006] found a total southward deep water transport of 17.5 Sv from a mean of four lowered ADCP sections. Previously, *Schott et al*. [2004] reported 12.9 Sv southward transport at the same latitude from mooring observations, the difference being attributed by the authors to the variability of the spatial extent and position of the current core not captured by the moorings in combination with a possible (under-)sampling by the LADCP sections. Based on these results, assuming a southward export of about 15 Sv at 42°N would require a minimum of 15 Sv of deep water with $\sigma_\theta > 27.68$ kg m^{-3} to return north between 42°N and 47°N, and contribute to the deep NAC. With the recirculation supplying about 45 Sv to the NAC transport, this leaves only a little fraction of about 5 Sv of northward deep water transport from subtropical origin (Figure 17).

The excess transport of the boundary current has to be carried north in the deep NAC, closing the subpolar gyre circulation that forms a very narrow loop southeast of Flemish Cap. This is clearly supported by the water mass properties. In our observations, the lateral salinity gradients in the LSW and uLSW that extend east of 42°W indicate that deep water from the DWBC recirculates in the NAC. Due to the horizontal uniformity, this is not so clear for the deeper water masses. This is in contrast to the situation at 42°N, where *Schott et al*. [2004] found a correlation between the NAC and the DWBC, but concluded on account of the water mass properties that the deep NAC there could not be regarded as an immediate recirculation of DWBC water.

The circulation pattern described here would imply that deep water from the boundary current is transferred into the interior of the subtropical gyre and the western basin of the subpolar Atlantic via the NAC/NBR system, which is in agreement with Lagrangian observations [e.g., *Bower et al*., 2009]. *Getzlaff et al*. [2006], using synthetic particles in an eddy resolving circulation model, found that due to intense eddy activity around the Grand Banks, about 40% of the deep water in the DWBC is diverted into the interior, spreading southward along the western flank of the Mid-Atlantic Ridge or with the eddying flow field in the basin interior. South of 47°N, an even higher drop of LSW transport was found from RAFOS and synthetic floats [*Bower et al*., 2009]. The Mann Eddy consistent with the circulation scheme presented here is stronger than found in earlier studies (based on earlier observations, e.g., *Meinen* [2001] suggested a Mann Eddy of 55 Sv). A weaker Mann Eddy would require a stronger northward NAC and less recirculation between 42 and 47°N. The southward transport observed within the NBR would then need to continue further south on interior pathways [e.g., *Bower et al*., 2009]. However, the similarity of the water mass properties observed at 47°N as well as the large-scale strong north-south gradients in chlorofluorocarbon distributions in the LSW layer [*Kieke et al*., 2007] do not support a strong connection between the Mann Eddy and the NAC/NBR circulation cell at 47°N.

6. Summary and Conclusions

Observations and model results show an alternating pattern of strong meridional currents east of Flemish Cap. Three major currents are located between 44° and 38°W, evident in repeated hydrography and altimetry as well as in the eddy-resolving VIKING20 ocean circulation model. Directly at the continental margin cold deep water masses from the Labrador Sea and the overflows are carried southward. The northward flowing North Atlantic Current is found farther offshore, followed in the east by its southward return flow. The transports of the main pathways are summarized in Figure 17; the observations are consistent with an overturning circulation of about 15 ±10 Sv, resulting from the mean difference between the northward NAC transport and the recirculation in the surface layer.

The deep western boundary current at 47°N has two distinct cores that are found in both observations and model, one with maximum at mid-depth, the other bottom intensified. This partitioning into two cores appears to be not uncommon; two cores were also observed farther south at the Grand Banks near 42°N [*Schott et al*., 2004], where the shallower core there had maximum velocities at about 1000 m depth, while the deep (bottom intensified) one was located at the 4300 m isobath, carrying the DSOW, and also at 53°N, where [*Fischer et al*., 2004] observed one shallow core near the surface, and one deep bottom intensified

core, with minimum velocities at about 1500 m depth in between. However, the two cores at 47° N exhibit different dynamics. The DWBC slope core is rather stable, but in the offshore direction the variability increases and (in the model) the bottom intensified DWBC rise core is strongly correlated to the NAC recirculation system on seasonal and longer timescales. South of 47° N, part of the DWBC makes a hairpin turn and returns northward within the NAC. The correlations in the model suggest that the return flow is mainly supplied by GFZW and DSOW from the DWBC rise core. This implies that at 47° N the LSW transport is less coupled to the circulation in the interior than the transport of overflow water masses.

Mesoscale processes like eddies play an important role for the freshwater budget of the subpolar gyre, because they supply a regular exchange of water with different salinities between the boundary current and the NAC. The differences in the T/S properties in the deep water in DWBC, NAC, and NBR, where the T/S of the NBR is closer to the boundary current than to the NAC, imply an exchange of heat and salt across the subpolar front in the Newfoundland Basin.

The timescales of the variability at 47° N of 20 to 50 days correspond to the earlier observations at 42° N, where 15 to 60 day periods were found [*Schott et al*., 2004, 2006]. In contrast, farther north within the subpolar gyre from Denmark Strait and at the boundary of the Labrador Sea, shorter timescales with 10 to 20 day period are dominant [*Fischer et al*., 2014].

The observed variability of the circulation ranges from synoptic to interannual; the coupling between the boundary and the interior makes it likely that the state of the circulation in the Newfoundland Basin determines the pathways of the NAC. The series of semi-permanent eddies between (and including) the Mann Eddy and the Northwest Corner is probably related to the number and position of branches crossing the Mid-Atlantic Ridge from the western to the eastern basin of the subpolar North Atlantic [*Bower and von Appen*, 2008], thereby possibly affecting the eastward flow of Iceland-Scotland-Overflow Water in the Charlie-Gibbs Fracture Zone [*Schott et al*., 1999], as well as mid-depth diapycnal mixing patterns at the Mid-Atlantic Ridge [*Walter and Mertens*, 2013].

Acknowledgments

We thank the captains and crews of the research vessels *Meteor*, *Maria S. Merian*, and *Thalassa* for able assistance. The altimeter products were produced by Ssalto/Duacs and distributed by Aviso with support from Cnes (http://www.aviso.oceanobs.com/duacs/), the model computations were performed at the North-German Supercomputing Alliance (HLRN). We thank three anonymous reviewers for their valuable comments. Observational and model data will be curated by the authors for at least 5 years after publication and made available to anyone upon request. This work was supported by the Cooperative Projects "Nordatlantik" (grants 03F0443C and 03F0605C, M. Rhein) and "RACE - Regional Atlantic Circulation and Global Change" funded by the German Federal Ministry for Education and Research (BMBF), and several grants by the Deutsche Forschungsgemeinschaft (DFG).

References

Behrens, E. (2013), The oceanic response to Greenland melting: The effect of increasing model resolution, dissertation, PhD thesis, Christian-Albrechts-Universität zu Kiel, Kiel. [Available at http://macau.uni-kiel.de/receive/dissertation_diss_00013684.]

Bower, A. S., and W.-J. von Appen (2008), Interannual variability in the pathways of the North Atlantic Current over the Mid-Atlantic Ridge and the impact of topography, *J. Phys. Oceanogr.*, *38*, 104–120.

Bower, A. S., B. Le Cann, T. Rossby, W. Zenk, J. Gould, K. Speer, P. L. Richardson, M. D. Prater, and H.-M. Zhang (2002), Directly measured mid-depth circulation in the northeastern North Atlantic Ocean, *Nature*, *419*, 603–607.

Bower, A. S., M. S. Lozier, S. F. Gary, and C. W. Böning (2009), Interior pathways of the North Atlantic meridional overturning circulation, *Nature*, *459*, 243–247.

Chelton, D. B., M. G. Schlax, R. M. Samelson, and R. A. de Szoeke (2007), Global observations of large oceanic eddies, *Geophys. Res. Lett.*, *34*, L15606, doi:10.1029/2007GL030812.

Debreu, L., C. Vouland, and E. Blayo (2008), AGRIF: Adaptive grid refinement in Fortran, *Comp. Geosci.*, *34*, 8–13.

Dengler, M., J. Fischer, F. A. Schott, and R. Zantopp (2006), Deep labrador current and its variability in 1996–2005, *Geophys. Res. Lett.*, *33*, L21S06, doi:10.1029/2006GL026702.

DRAKKAR Group (2007), Eddy-permitting ocean circulation hindcasts of past decades, in *CLIVAR Exchange No. 42*, vol. 12(3), pp. 8–10, Int. CLIVAR Proj. Off., Southampton, U. K.

Egbert, G., and S. Erofeeva (2002), Efficient inverse modeling of barotropic ocean tides, *J. Atmos. Oceanic Technol.*, *19*, 183–204.

Fichefet, T., and M. A. M. Maqueda (1997), Sensitivity of a global sea ice model to the treatment of ice thermodynamics and dynamics, *J. Geophys. Res.*, *102*(C6), 12,609–12,646, doi:10.1029/97JC00480.

Fischer, J., F. A. Schott, and M. Dengler (2004), Boundary circulation at the exit of the Labrador Sea, *J. Phys. Oceanogr.*, *34*, 1548–1570.

Fischer, J., M. Visbeck, R. Zantopp, and N. Nunes (2010), Interannual to decadal variability of outflow from the Labrador Sea, *Geophys. Res. Lett.*, *37*, L24610, doi:10.1029/2010GL045321.

Fischer, J., et al. (2014), Intra-seasonal variability of the deep western boundary current in the western subpolar north Atlantic, *Prog. Oceanogr.*, in press, doi:10.1016/j.pocean.2014.04.002.

Gary, S. F., M. S. Lozier, C. W. Böning, and A. Biastoch (2011), Deciphering the pathways for the deep limb of the meridional overturning circulation, *Deep Sea Res., Part II*, *58*, 1781–1797.

Getzlaff, K., C. W. Böning, and J. Dengg (2006), Lagrangian perspectives of deep water export from the subpolar North Atlantic, *Geophys. Res. Lett.*, *33*, L21S08, doi:10.1029/2006GL026470.

Hogg, N. G. (1992), On the transport of the Gulf Stream between Cape Hatteras and the Grand Banks, *Deep Sea Res., Part A*, *39*, 1231–1246.

Käse, R. H., and W. Krauss (1996), The Gulf stream, the north Atlantic Current, and the origin of the Azores Current, in *The Warmwatersphere of the North Atlantic Ocean*, edited by W. Krauss, pp. 291–337, Gebrüder Borntraeger, Berlin, Stuttgart.

Kieke, D., M. Rhein, L. Stramma, W. M. Smethie, J. L. Bullister, and D. A. LeBel (2007), Changes in the pool of Labrador Sea Water in the subpolar North Atlantic, *Geophys. Res. Lett.*, *34*, L06605, doi:10.1029/2006GL028959.

Kieke, D., B. Klein, L. Stramma, M. Rhein, and K. Koltermann (2009), Variability and propagation of Labrador Sea Water in the southern subpolar North Atlantic, *Deep-Sea Res., Part I*, *56*, 1656–1674.

Krauss, W. (1986), The North Atlantic current, *J. Geophys. Res.*, *91*(C4), 5061–5074, doi:10.1029/JC091iC04p05061.

Large, W. G., and S. G. Yeager (2008), The global climatology of an interannually varying air-sea flux data set, *Clim. Dyn.*, *33*, 341–364.
Lazier, J. R. N. (1994), Observations in the northwest corner of the North Atlantic Current, *J. Phys. Oceanogr.*, *24*, 1449–1463.
Lozier, M. S., S. F. Gary, and A. S. Bower (2013), Simulated pathways of the overflow waters in the North Atlantic: Subpolar to subtropical export, *Deep Sea Res., Part II*, *85*, 147–153.
Lumpkin, R., K. G. Speer, and K. P. Koltermann (2008), Transport across 48°n in the Atlantic Ocean, *J. Phys. Oceanogr.*, *38*, 733–752.
Madec, G. (2008), NEMO ocean engine, *Tech. Rep. 27*, Inst. Pierre-Simon Laplace (IPSL), Paris.
Mann, C. R. (1967), The termination of the Gulf Stream and the beginning of the North Atlantic Current, *Deep Sea Res. Oceanogr. Abstr.*, *14*, 337–359.
Meinen, C. S. (2001), Structure of the North Atlantic Current in stream–coordinates and the circulation in the Newfoundland Basin, *Deep Sea Res., Part I*, *48*, 1553–1580.
Meinen, C. S., and D. R. Watts (2000), Vertical structure and transport on a transect across the North Atlantic Current near 42°N: Time series and mean, *J. Geophys. Res.*, *105*(C9), 21,869–21,891, doi:10.1029/2000JC900097.
Reverdin, G., P. P. Niiler, and H. Valdimarsson (2003), North Atlantic Ocean surface currents, *J. Geophys. Res.*, *108*(C1), 3002, doi:10.1029/2001JC001020.
Rhein, M., J. Fischer, W. M. Smethie, D. Smythe-Wright, R. F. Weiss, C. Mertens, D.-H. Min, U. Fleischmann, and A. Putzka (2002), Labrador Sea Water: Pathways, CFC inventory, and formation rates, *J. Phys. Oceanogr.*, *32*, 648–665.
Rhein, M., D. Kieke, S. Hüttl-Kabus, A. Roessler, C. Mertens, R. Meissner, B. Klein, C. W. Böning, and I. Yashayaev (2011), Deep water formation, the subpolar gyre, and the meridional overturning circulation in the subpolar North Atlantic, *Deep Sea Res., Part II*, *58*, 1819–1832.
Roessler, A. (2013), Observed subpolar gyre transports at the Mid-Atlantic Ridge, dissertation, PhD thesis, Univ. Bremen, Bremen. [Available at http://nbn-resolving.de/urn:nbn:de:gbv:46–00103001-19.]
Rossby, T. (1996), The North Atlantic Current and surrounding waters: At the crossroads, *Rev. Geophys.*, *34*(4), 463–481, doi:10.1029/96RG02214.
Schmitz, W. J., Jr., and M. S. McCartney (1993), On the North Atlantic circulation, *Rev. Geophys.*, *31*(1), 29–49, doi:10.1029/92RG02583.
Schott, F., L. Stramma, and J. Fischer (1999), Interaction of the North Atlantic Current with the deep Charlie Gibbs fracture zone throughflow, *Geophys. Res. Lett.*, *26*, 369–372, doi:10.1029/1998GL900223.
Schott, F. A., R. Zantopp, L. Stramma, M. Dengler, J. Fischer, and M. Wibaux (2004), Circulation and deep–water export at the western exit of the subpolar North Atlantic, *J. Phys. Oceanogr.*, *34*, 817–843.
Schott, F. A., J. Fischer, M. Dengler, and R. Zantopp (2006), Variability of the Deep Western Boundary Current east of the Grand Banks, *Geophys. Res. Lett.*, *33*, L21S07, doi:10.1029/2006GL026563.
Smethie, W. M., Jr., R. A. Fine, A. Putzka, and E. P. Jones (2000), Tracing the flow of North Atlantic Deep Water using chlorofluorocarbons, *J. Geophys. Res.*, *105*(C6), 14,297–14,323, doi:10.1029/1999JC900274.
Stramma, L., D. Kieke, M. Rhein, F. Schott, I. Yashayaev, and K. P. Koltermann (2004), Deep water changes at the western boundary of the subpolar North Atlantic during 1996 to 2001, *Deep Sea Res., Part I*, *51*, 1033–1056.
Visbeck, M. (2002), Deep velocity profiling using lowered acoustic Doppler current profilers: Bottom track and inverse solutions, *J. Atmos. Oceanic Technol.*, *19*, 794–807.
Walter, M., and C. Mertens (2013), Mid–depth mixing linked to North Atlantic current variability, *Geophys. Res. Lett.*, *40*, 4869–4875, doi:10.1002/grl.50936.
Xu, X., H. E. Hurlburt, W. J. Schmitz, Jr., R. Zantopp, J. Fischer, and P. J. Hogan (2013), On the currents and transports connected with the Atlantic meridional overturning circulation in the subpolar North Atlantic, *J. Geophys. Res.*, *118*, 502–516, doi:10.1002/jgrc.20065.